University of Tripoli
Faculty of Engineering
Aeronautical Engineering Department

GPA of CF6-80C2 Engine Performance Prediction with GSP Program

By

Mahmud Mohamed Ghouma Marwan

Supervised By

Dr. Prof. Aiman Elmahmodi

This Thesis Submitted in Partial Fulfilment of the Requirement of Masters of Science Degree in Aeronautical Engineering

Tripoli -Libya

Spring - 2022

ACKNOWLEDGEMENT

All thanks to Allah, Lord of the worlds, who created me and provided me with the means of knowledge. I would like to convey my heartfelt gratitude to my supervisor Prof. Dr. Aiman Elmahmodi for his tremendous direction, advice, and assistance from the beginning to the completion of my thesis, even in my postgraduate study.

I would like to express my special thanks to Mr. Eng. Oscar Kogenhop, who works at the Netherlands Aerospace Centre, a member of the GSP Team, for his time and efforts. Your useful suggestions were really helpful.

Thanks to all Professors and Doctors, who teach me scientific subjects during my postgraduate study, and all team of the Aeronautical Engineering Department. Thank you to my colleagues at Libyan Airlines who helped me with technical matters.

I am most grateful to my parents, mother, and to my father (Teacher Mohamed Ghouma Marwan), who taught me to love and care about sciences, May Allah have mercy on him, that had passed away last year. Thanks a lot to my wife, my son Ali, to my brothers and sisters.

I dedicate this thesis to my father, who would love to see this work. May Allah forgive him and have mercy on him.

ABSTRACT

Gas turbine engines deteriorate over time; their performance will change. Using GPA, the degraded component can be identified, after which corrective steps can be taken. In this thesis, GPA has been performed by using the GSP, which has modern capabilities to analyze the performance of the CF6-80C2 engine model.

CF6-80C2 engine model was created by using GSP, based on test cell measurements data that have been taken from the references, and by adapting the model to the test cell data according to adapting procedures, and some assumptions made due to lack of information about the engine. The Take-off power setting has been chosen as a design point of the engine model. Off-design performance simulation was built in GSP, based on generic components maps that have been scaled to match the measured CF6-80C2 performance design point, describing the performance of the compressors and turbines of the engine model.

The deterioration simulations assumptions on the CF6-80C2 engine model have been applied in GSP, by changing the corrected mass flow rate and isentropic efficiency of the engine components. Seven deterioration cases have been studied, which have been divided into two categories, the first one has studied single-component deterioration, and its effect on all engine components, and the other one has studied combined component deterioration. The results of the studied cases have been shown in bar chats, to present the percentage changes in the pressure and temperature of each engine station, N2 speeds, fuel flow, and thrust, and GSP charts to present the changes in the pressure ratios and temperature ratios with changes of corrected mass flow rate and isentropic efficiency of the engine components. EGT margin of the engine deteriorated cases have been studied and plotted. The results of the CF6-80C2 GSP engine model have been compared with a case study of the GPA exponential data of the test cell for CF6-80C2 from [2]. The comparison between the GSP model and GPA experimental data shows very good agreement, staying with +/- 0.39% as the maximum difference range for all measured engine parameters that are compared.

خلاصة المشروع:

أداء المحركات التوربينية النفاثة يتدنى مع مرور الوقت, هذا التدني في الأداء يمكن قياسه ومعرفته من خلال تحليل مسار الهواء والغاز GPA, حيث باستخدام GPA يمكن معرفة المكون متدني الأداء (أحد مكونات المحرك) بعدها يمكن اتخاذ الخطوات التصحيحية لمعالجة هذا التدني في الأداء.

تم إنشاء نموذج محاكاة أداء محرك CF6-80C2 باستخدام برنامج محاكاة التوربينات الغازية (GSP), بناءا على قياسات وبيانات عملية للمحرك (Test Cell Data), والتي تم الحصول عليها من بعض المراجع, ومن خلال تعديل بيانات نموذج أداء المحرك مع البيانات العملية, وبعض الفرضيات التي تم إتخاذها بسبب قلة المعلومات العملية حول أداء المحرك. تم اختيار نقطة تصميم النموذج عند طاقة الإقلاع (Take-off Power). تم بناء نموذج محاكاة الأداء خارج نقطة التصميم (Off-Design) في برنامج GSP بناءا على رسومات بيانية عامة لمكونات المحرك (Generic Component Maps), التي تم تعديلها في برنامج GSP لتتناسب مع نقطة تصميم المحرك, لتصف أداء الظواغط (LPC, HPC) والتوربينات (LPT, HPT) الخاصة بالمحرك.

تم تطبيق فرضيات لتدني الأداء على نموذج المحرك CF6-80C2 في برنامج GSP وذلك من خلال تغيير معدل تدفق الغاز (W_C) و الكفاءة (η) لعدد من مكونات المحرك. تم دراسة سبعة حالات لتدني أداء المحرك حيث تم تقسيمها إلى فئتين, الفئة الأولى درست حالات تدني أداء مكون واحد ومدى تأثيره على كل مكونات المحرك , والفئتة الثانية درست تدني أداء أكثر من مكون في نفس الوقت. تم عرض نتائج حالات تدني أداء المحرك المدروسة عن طريق الرسومات البيانية (Bar Charts)، لعرض نتائج النسبة المئوية للتغيرات في (الضغط P ودرجة الحرارة T لكل مكون من مكونات المحرك ، وسرعات N2 ، وتدفق الوقود Wf ، وقوة دفع المحرك FN)، وعن طريق الرسومات البيانية لبرنامج GSP لعرض نتائج (التغيرات في نسب الضغط ودرجة الحرارة لمكونات المحرك مع التغيرات في معدل تدفق الغاز (W_C) والكفاءة (η) لمكونات المحرك) .تم دراسة البارامیتر (EGT Margin) الخاص بحالات تدني أداء المحرك المدروسة وتم عرض النتائج في الرسومات البيانية (Bar Chart). تمت مقارنة نتائج نموذج أداء محرك CF6-80C2 بنتائج دراسة تجريبية (Test Cell Results) من المرجع [2], أجريت للمحرك CF6-80C2. أظهرت نتائج المقارنة بين نموذج GSP وبيانات GPA التجريبية توافقًا جيدًا للغاية ، حيث أن أقصى فارق هو في حدود (+/- 0.39٪) لجميع بارامترات المحرك المقاسة التي تمت مقارنتها.

TABLE OF CONTENTS

LIST OF FIGURES

LIST OF TABLES

NOMENCLATURE

AM	Adaptive Modelling
ANN	Artificial Neural Network
BPR	Bypass Ratio
DOD	Domestic Object Damage
EGT	Exhaust Gas Temperature
EEC	Engine Electronic Control
FADEC	Full Authority Digital Engine Control
FN	Net Thrust
FCM	Fault-Correlation Matrix
FOD	Foreign Object Damage
GA	Genetic Algorithm
GE	General Electric
GPA	Gas Path Analysis
GSP	Gas Turbine Simulation Program
GUI	Graphical User Interface
HPC	High Pressure Compressor
HPT	High Pressure Turbine
ICM	Influence-Coefficient Matrix
IGV	Inlet Guide Vane
ISA	International Standard Atmosphere
KLM	Royal Dutch Airlines
KLM ES	KLM Engine Services
LPC	Low Pressure Compressor
LPT	Low Pressure Turbine
MC	Maximum Continuous

NLR	Netherlands Aerospace Centre
OEM	Original Equipment Manufacturer
OPR	Overall Pressure Ratio
PR	Pressure Ratio
SFC	Specific Fuel Consumption
VBV	Variable Bleed Valve
VSV	Variable Stator Vane

Roman symbols

A	Area [m^2]
C_P	Specific Heat at Constant Pressure [kJ/kg/K]
D	Characteristic Linear Dimension [m]
F	Force [N]
h	Enthalpy [J]
M	Mach Number [-]
$\dot{m}$	Mass Flow [kg/s]
p	Pressure [Pa] or [Bar]
R	Specific Gas Constant [J/ kg.k]
T	Temperature [K] or [C°]
v	Velocity [m/s]
N	Rotational Speed [rpm]
P_S	Static Pressure [Pa] or [Bar]
P_0, Pt	Total Pressure [Pa]
RHUM	Relative Humidity [%]
Tt, T_0	Total temperature [K] or [∘C]
W	Mass Flow [kg/s]
WF	Fuel Flow [kg/s]
WA2	Total Engine Mass Flow [kg/s]

Greek symbols

γ	Ratio of Specific Heats [-]
$\mathbf{\Delta}$	Difference
δ	Normalised Pressure [-]
η	Efficiency [-]
θ	Normalised Temperature [-]
ρ	Density [kg/m^3]

Subscripts

0,	Total Property
1, 2, 25...	Engine Station Numbering
a	Ambient
c	Compressor
c	Corrected
cc	Combustion
f	Fuel
g	Gas
is	Isentropic
j	Jet
m	Mechanical
t	T

CHAPTER 1

INTRODUCTION

1.1 OVERVIEW

Operational aero-engines are high-priced machines, that require periodic and specialized maintenance to maintain them in working order, which is essential for safe, reliable, and cost-effective aircraft operations. Aero engines like any gas turbine engine deteriorate over time, and their performance will change, which affects their aerothermodynamics and mechanical performance. The changes in aero engine performance can be measured in the gas path of the engine by Gas Path Analysis (GPA).

Gas path analysis (GPA) is a performance diagnostic method that can identify engine modules responsible for engine performance problems without the need for engine removal or disassembly [2]. GPA relates to the variation of engine performance parameters which results from engine deteriorations, so that, using GPA the degraded component in a gas turbine engine can be identified.

Gas Turbine engine modeling techniques and simulations have become increasingly important as computers have improved. The modeling may be presented as a mathematical model description, representing the physical behavior of the engine. This can be done in either 0-D, 1-D, 2-D, and 3-D [9].

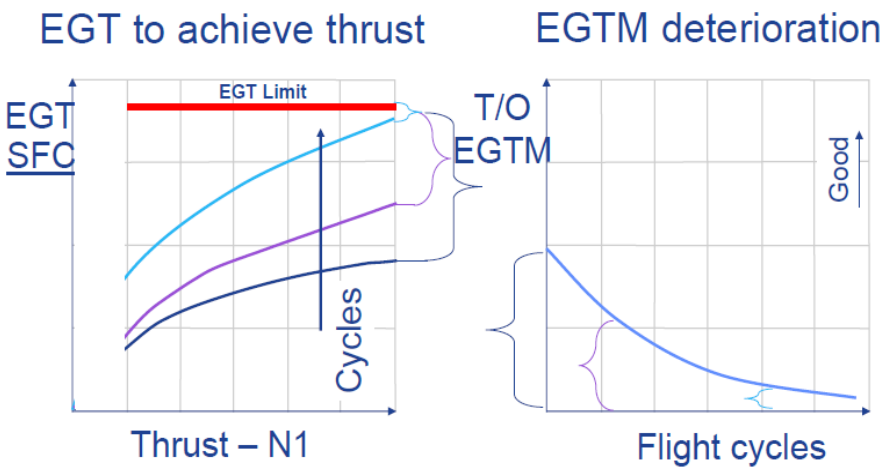

Figure (1.1): EGTM to Measure Engine Performance Deterioration [11]

The most important performance parameter in aero-engines is Exhaust Gas Temperature (EGT). Each engine has an EGT redline is established, an EGT that can't be exceeded [1]. Figure (1.1) shows how EGT margin decreases with increases in flight cycles.

1.2 BACKGROUND INFORMATION ON GSP

Analyzing and study of the performance of different gas turbine engines has arisen from different gas turbine engines operators, and due to the difficulty of getting the performance analysis information outside OEM, which thrusted the developers of commercial programs to start programming mathematical models of gas turbine engines such as GasTurb, and GSP [2].

The GSP has a user-friendly interface, allowing quick implementations of gas turbine engine models and quick analysis of complex problems [3]. Figure (1.2) shows the GSP model of a twin-spool turbofan engine.

GSP is described as a graphical user interface that fully reflects the object-oriented architecture of the gas turbine system and component models

[3]. GSP can be described as a 0-D simulation program [3], where the flow properties are only calculated at the inlet and outlet of the components [2].

GSP is powerful for performance prediction of design points, and off-design analysis of any gas turbine engine, even the steady state and transient simulations of any gas turbine engine can be described. Also, deteriorations can be modeled in GSP as an off-design condition.

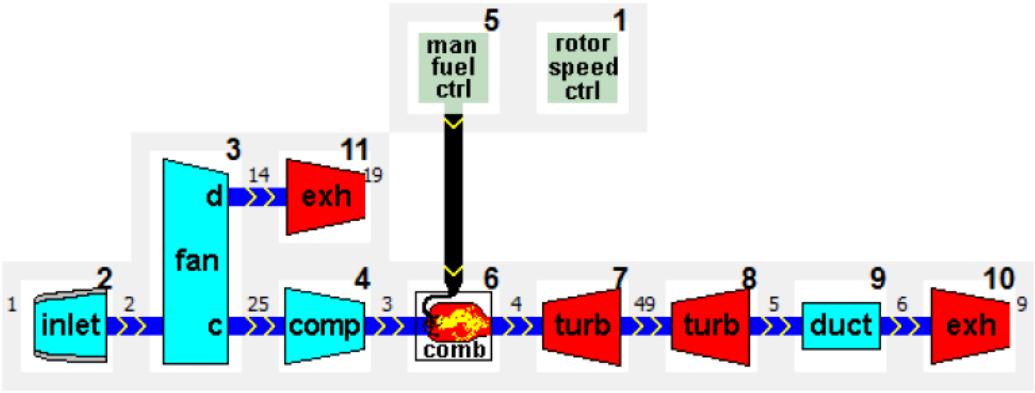

Figure (1.2): GSP Model of a Twin-Spool Turbofan Engine [3]

GSP started at the Delft University of Technology and the Netherlands Aerospace Centre in 1986 [3]. NASA's DYNGEN program was used for Jet and Turbofan engine simulations [3]. The program has been rewritten in FORTRAN77 at NLR and finally in Borland Delphi for use on Microsoft Windows computers [1, 3].

1.3 COMPONENT PERFORMANCE OVERVIEW

The first study of the performance of the gas turbine engine model is a prediction of the design point of the engine model aimed to study. Which are the condition, ambient condition, and power setting at which all the engine its components run at their design operating point [9]. That is the speed, pressure

ratio, and mass flow for which the components of a gas turbine are designed [9].

After fixing the design point of a gas turbine engine, off-design computations may be started, which have widely varying operating characteristics. Off-design performance of gas turbine engine components can be specified by using components maps [2]. Where the compressors and turbines are described visually using compressor and turbine maps, which present the variation of mass flow, pressure ratio, and efficiency with the rational speed of the compressors and turbines.

Components characteristics maps are tabulated in GSP, which is stored in separate files. The following parameters are generally used for component maps, which will be described.

1. **Pressure Ratio**

$PR = \frac{P_{out}}{P_{in}}$ (for the Compressor), $PR = \frac{P_{in}}{P_{out}}$(for the Turbine)……(1.1)

2. **Isentropic Efficiency**

$\eta_{is} = \frac{\Delta h_{is}}{\Delta h_{real}}$ (for compressor) , $\eta_{is} = \frac{\Delta h_{real}}{\Delta h_{is}}$ (for Turbine)…..…(1.2)

Where, $\Delta h_{is} = C_P \Delta T_{is}$, and $\Delta h_{real} = C_P \Delta T_{real}$

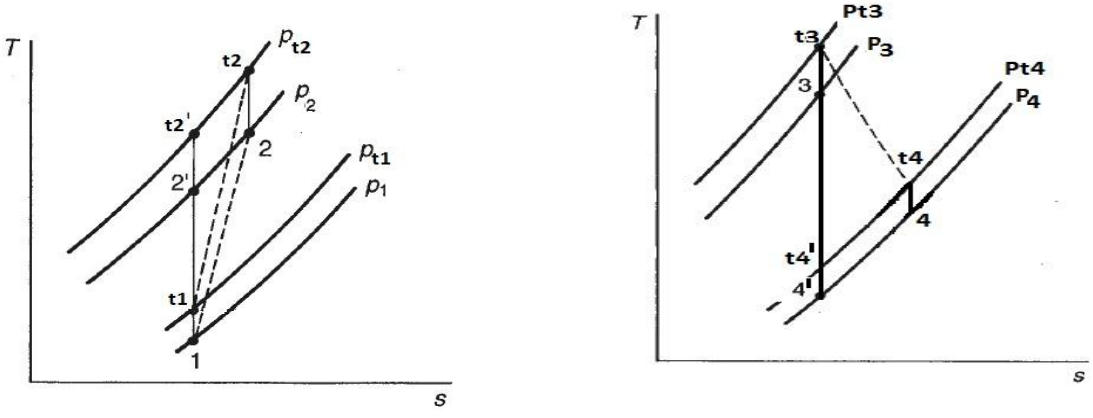

Figure (1.3): Isentropic and Real Parameters for Compressor and Turbine Respectively

Equation (1.2) represents generic isentropic relations of the compressors and turbines. Figure (1.3), shows the real and isentropic parameters for the compressor and turbine respectively, where for the compressor, it's assumed that (t1) is the inlet total condition, (t2) is outlet total condition, while for the turbine, (t3) is the inlet total condition, (t4) is the outlet total condition. The numbers in figure (1.3) are just for the general view.

3. Corrected Mass Flow Rate

$$W_c = \frac{W\sqrt{\frac{T}{T_{ref}}}}{\frac{P}{P_{ref}}} = \frac{W\sqrt{\theta}}{\delta} \quad \text{..... (1.3)}$$

$\theta = T/T_{amb}$ and $\delta = P/P_{amb}$

Where the reference values of the temperature and pressure in the model will be as these values: $T_{ref} = 289\ k$ and $P_{ref} = 1.011\ bar$, while T, P, and w (mass flow), refer to inlet total parameter entering the component.

4. Corrected Speed

$$N_c = \frac{\frac{N}{N_{ref}}}{\sqrt{\frac{T}{T_{ref}}}} = \frac{\frac{N}{N_{ref}}}{\sqrt{\theta}} \quad \text{..... (1.4)}$$

Note that the corrected spool speeds used in the component characteristic maps for compressors and turbines in GSP use the following relation in equation (1.5) [3], without a reference spool speed the relation becomes equation (1.5) [3].

$$N_c = \frac{N}{\sqrt{\theta}} \quad \text{..... (1.5)}$$

5. Reynolds Number

The Reynolds number is required for full specification of component performance [2]. It is a measure of the ratio of inertia forces to viscous forces and quantifies the relative importance of these two forces for given flow conditions [2]. The greatest effect of Reynolds number variations, as a result

of altitude changes, is on component efficiency. However, performance effects due to Reynolds number variations are small and therefore neglected in most cases [2].

Table (1.1) : Parameter Groups Used for Gas Turbine Performance Analysis [1]

Performance Parameters	**Dimensionless Parameters**	**Quasi-Dimensionless Parameters**	**Corrected Parameters**
Pressure Ratio	$\frac{P_{02}}{P_{01}}$	$\frac{P_{02}}{P_{01}}$	$\frac{P_{02}}{P_{01}}$
Efficiency	η	η	η
Mass Flow	$\frac{\dot{m}\sqrt{R\,T_{01}}}{P_{01}\,D^2}$	$\frac{\dot{m}\sqrt{T_{01}}}{P_{01}}$	$\frac{\dot{m}\sqrt{\theta}}{\delta}$
Rotational Speed	$\frac{N\,D}{\sqrt{R\,T_{01}}}$	$\frac{N}{\sqrt{T_{01}}}$	$\frac{N}{\sqrt{\theta}}$

Table (1.1) shows Non-dimensional and corrected parameters used for component performance. The working medium in a specific gas turbine configuration is fixed. Therefore, the universal gas constant *R*, shown in the

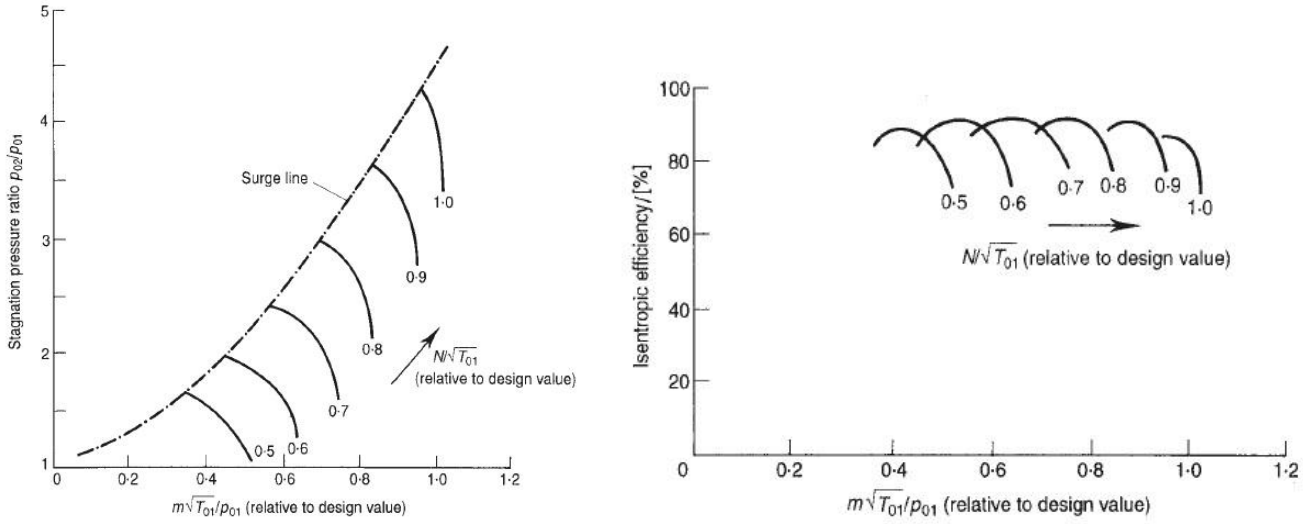

Figure (1.4): Example of a Generic Axial Compressor Map [5]

non-dimensional group of the mass flow and shaft rotational speed, is often omitted. If a specific compressor design is analyzed, the characteristic geometry *D* will remain constant and can therefore be omitted [2].

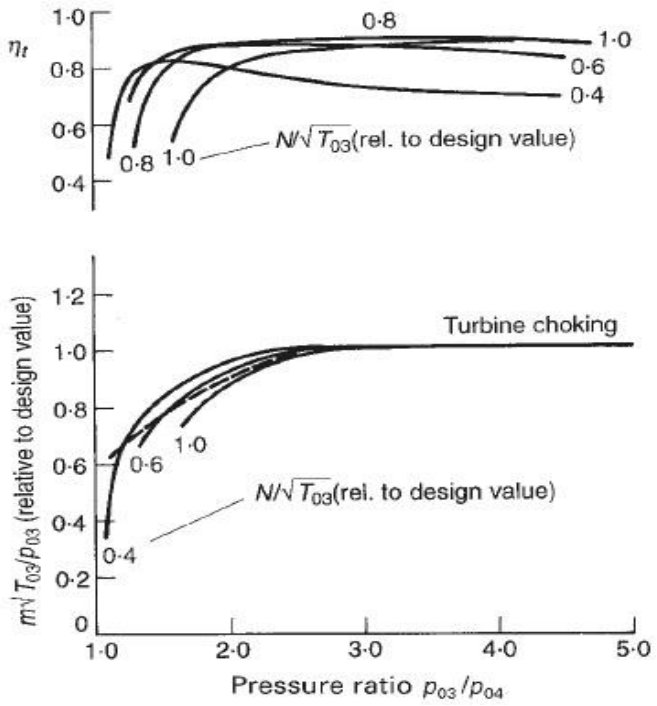

Figure (1.5): Example of a Generic Axial Turbine Map [5]

The component maps are proprietary to the OEM and are therefore not publicly available. When a model is created of an existing engine these maps have to be reverse-engineered, by tuning publicly available maps until they match the measured performance on the actual engine [1]. This process will not be described in this thesis. Figures (1.4) and (1.5) show the generic axial compressor and turbine maps respectively.

1.4 CF6-80C2 ENGINE SPECIFICATIONS

1.4.1 OVERVIEW

The engine to be modeled in GSP in this thesis is General Electric CF6-80C2. The CF6-80C2 high-bypass turbofan engine combines a proven core with modern technical innovations to offer the highest reliability, longest life, and lowest fuel burn in its thrust class [8].

Technologies from a variety of research and development programs (including the GE/NASA Energy Efficient Engine program) have been incorporated into the CF6-80C2 design, such as advanced cooling techniques to improve overall efficiency, advanced clearance control, and aerodynamic modifications of blades and vanes [8].

The engine entered revenue service in October 1985 and has consistently demonstrated the lowest specific fuel consumption of any large commercial transport engine in its thrust class [8]. Currently certified on 14 widebody aircraft models and with 16 ratings, the CF6-80C2 has received FAA 180-minute Extended Range Operations (ETOPS) approval for A300, A310, B747, and B767 aircraft, offering route structuring flexibility and added economic benefits [8]. The engine is controlled electronically by the Engine Electronic Control system (EEC), which is a Full Authority Digital Engine Control (FADEC) [18]. Another version of CF6-80C2 shown in table (A.1) in Appendix (A), will not be modeled or researched in this thesis.

Figure (1.6): CF6-80C2 Picture [8]

1.4.2 LAYOUT AND SYSTEMS OF CF6-80C2 ENGINE

Figure (1.6) shows a general outside view of the engine, and figure (1.7) shows more detail of the inside of the engine, which are the component's positions of the engine are shown. The engine primary specifications are shown in table (1.2).

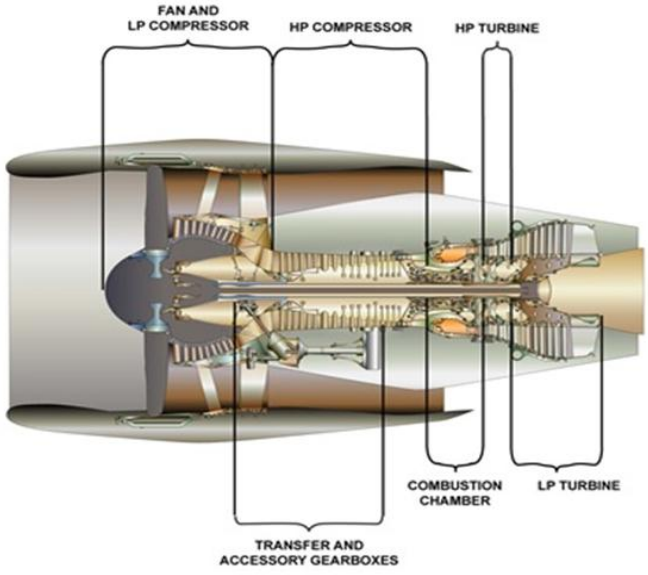

Figure (1.7): Layout of the CF6-80C2

Table (1.2): CF6-80C2 Characteristics and Components [18]

Characteristics	**Components**
LPC	1 Fan + 3 Primary Stages
HPC	14 Primary Stages
HPT	2 Primary Stages
LPT	5 Primary Stages
Max Diameter	(106 in) (269 cm)
Length	(168 in) (427 cm)
Dry Weight	(9480–9860)lb. (4300 - 4472) kg
Overall Pressure Ratio at Maximum Power	27.1 – 31.8
Bypass Ratio	5 - 5.31

In the intake of the engine, the airflow enters the fan with uniform pressure and velocity. In the fan, the airflow is split into the bypass and core. About five times much mass airflow goes through the bypass, again exiting the core engine [20].

The core airflow travels through the booster (LPC) and HPC, where the pressure is increased approximately 31 times [20]. Next, the combustion chamber heat is added to the flow (air and fuel), which is extracted in HPT and LPT. After this the core flow exit the engine. The fan and booster, and LPT are connected to the N1 shaft, and the HPC and HPT are connected to the N2 shaft and are considered the core engine.

The fan of the engine is consisting of 38 blades, designed of solid titanium [17], which is responsible for the largest part of the thrust produced by the engine. The booster consists of three stages, located behind the fan.

Behind the booster Variable Bleed Valves (VBVs) are installed, allowing for a reduction in mass flow going toward the HPC [18].

The core engine starts with the HPC, which consists of 14 stages, the stators of the first 5 stages are variable stator vanes (VSV) to minimize fuel consumption and to control engine stall margin and change stator vanes angle depending on the engine operating regime [18]. The HPC is responsible for the largest part of the pressure rise in the engine.

The hot section starts with the combustion chamber, followed by 2 stages of HPT, and 5 stages of LPT. In order to optimize engine fuel consumption and minimize deterioration, the HPT and LPT are cooled externally with air bled from the HPC [18]. Through control valves managed by the main engine control (MEC) OR (FADEC) [18].

1.5 THESIS OBJECTIVES AND QUESTIONS

The objective of this thesis is to study GPA to the CF6-80C2 engine performance by creating the engine model in GSP which is capable of providing accurate GPA results for that engine.

The overall research questions can be summarized as: How can the Gas Path Analysis with Gas Turbine Simulation Program be applied to the CF6-80C2? And, Is the created model providing accurate and usable GPA results?

1.6 THESIS STRUCTURE

This thesis will be divided into six chapters, Chapter 1 and Chapter 2 contains necessary background information, giving the theoretical background of the thesis. This is followed by Chapter 3 to Chapter 6 in which

the GSP model of the engine CF6-80C2 is created and discussed, which is followed by a conclusion and recommendations.

Chapter 2 describes gas turbine deterioration, deterioration mechanisms, and effects of component degradation. And gas path analysis concept, with an overview of GPA methods.

In **Chapter 3** the model of CF6-80C2 was created, followed by design point modeling.

In **Chapter 4** off design model is created with engine component maps by GSP.

In **Chapter 5** simulated deteriorations are applied to the model to investigate the component degradation.

The thesis is concluded in **Chapter 6**, where the recommendations will be given as well.

CHAPTER 2

GAS TURBINE DETERIORATION AND GPA CONCEPT

2.1 LITERATURE SURVEY

Gas turbine engine's performance prediction methods and maintenance strategies are as old as the gas turbine engines themselves and have evolved considerably over time.

A few articles describe field experience with GPA in the aero-engine maintenance process [2]. The research about this topic in the late 1970s and early 1980s have led to the development of several GPA tools from the gas turbine original equipment manufacturers (OEMs) such as TEMPER, developed by General Electric, and COMPASS, developed by Rolls Royce [2]. These methods were a considerable step forward in the field of gas path diagnostics, but their accuracy was not always sufficient for maintenance applications [2]. Since then the research in this field has been mainly focused on improving the accuracy of GPA methods [2].

Several publications describe engine performance deteriorations and engine diagnostics using GPA techniques, such as a pertinent generic computer program called PYTHIA has been developed for the JT9D engine [22]. Sallee, and Sallee et al devised mathematical models to predict the reductions in flow capacity and efficiencies of engine components, such as the

LPC, HPC, LPT, and HPT, arising due to faults such as increased tip-clearance or airfoil erosion [22].

2.2 DETERIORATION OVERVIEW

Any gas turbine engine and any machine are not immune to deterioration. The deterioration is a loss in engine performance due to the mechanical degradation of components [9].

The severity of component degradation can be represented by the difference between the actual component condition parameters and their baseline values. This difference is referred to as the condition delta or component condition deviation. Large condition deltas represent more severe deterioration, and equation (2.1) represents how to calculate condition delta (Δ), or component condition deviation [15].

$$\Delta = \frac{Observed\ Value - Baseline\ Value}{Baseline\ Value} * 100 \quad \text{(2.1)}$$

Following the deterioration mechanisms, the effect of deterioration on each individual component will be described.

2.2.1 FOULING

Fouling can be identified as the degradation of flow capacity and efficiency caused by the adherence of particulate contaminates to the gas turbine airfoil and annulus surfaces [15]. Although fouling can occur in both compressor and turbine components, it has been recognized that compressor fouling is one of the most common causes of engine performance deterioration [15]. Gas turbines are particularly susceptible to fouling because of the large quantities of air they ingest. The incoming air consists of hard and soft particles as it is shown in figure (2.2). The fouling is worsened if there is an

oil leak, because oil can as glue, especially at the later stages of the compressor [15]. Fouling causes to change in the aerodynamic shape, and inlet angle of the airfoil, which increases surface roughness and reduces the airfoil throat opening [15]. In some cases, the performance deterioration due to fouling can often be recovered by washing or cleaning the engine.

The effect of fouling on compressor flow capacity is more significant than the effect on efficiency. Typically, due to compressor fouling, the flow capacity is reduced by 3-8% and efficiency by 1% depending on the severity of the fouling [15].

The reduction in mass flow capacity varies with operating speed, ambient temperate, and altitude [15]. Furthermore, compressor fouling also reduces the compressor surge margin and this may result in compressor surge. Previous studies on compressor fouling suggest that a reduction in flow capacity should be coupled with an equal reduction in compressor pressure ratio [15].

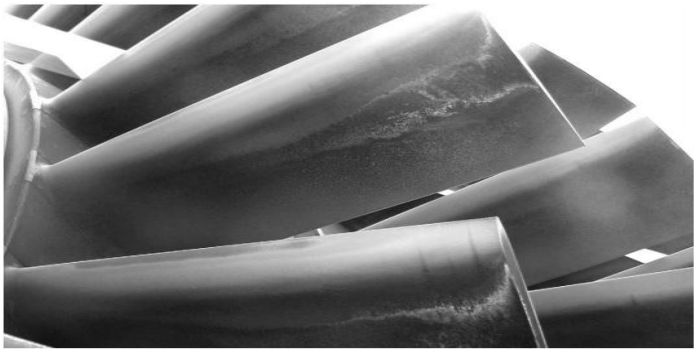

Figure (2.1): Deposits on a Compressor Rotor Blades, (Fouling) [13]

In the case of the turbine nozzle guide vane fouling, the effective nozzle area (and therefore the turbine flow capacity) is reduced and so is the turbine isentropic efficiency. The effect on turbine nozzle area change is less significant than the flow capacity change in the fouled compressor. Typically,

the efficiency is reduced by 1% [15]. No published figure is available for the flow capacity increase but it can be assumed that it will be of the order of 2% [15].

2.2.2 ABRASION

Abrasion is the removal of material by rubbing two surfaces together. This can occur in gas turbines when a rotating surface rubs over a non-rotating surface [1]. Abrasion leads to increased tip clearances. Increased tip clearances lead to unwanted tip flows, leading to a loss in efficiency, mass flow, pressure ratio in compressors, and work output in turbines [1]. So due to tip clearances the difference between casing radius and the blade tip radius would be increased, which greatly impacts component performance (+1% tip clearance results in -2% efficiency), reduces flow capacity of the component, and Increases over time [15]. Figure (2.2) shows an example of tip clearance between rotating blade and the casing of a compressor.

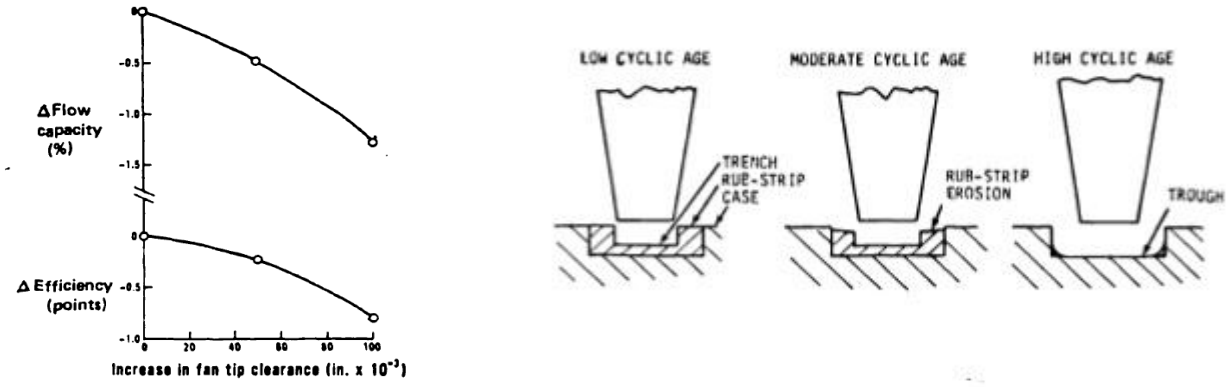

Figure (2.2): Tip Clearance Changes of Typical LPC [11]

2.2.3 EROSION

Larger particles entering the gas turbine will remove material from the surfaces they hit [1]. This process is called erosion. Figure (2.3) shows an example of erosion in a compressor blade. Erosion, causes an increase in surface roughness, changes in shapes, and increased tip clearances.

Erosion of the compressor is more significant at the later stages, as pressures increase [1]. In the compressor, erosion will lead to decreased pressure ratios and mass flow, while also leading to a decreased surge margin at the earlier stages [1]. In the turbine erosion may lead to an increase in mass flow, if the material is removed at the inlet, performance however will decrease [1].

For both, compressor and turbine erosion, the effect on flow capacity is greater than the effect on efficiency. Typically, flow capacity for the turbine is increased by 2%, and efficiency is decreased by 1% [15]. No figure is available for the compressor flow capacity decrease but it can be assumed that it will be of the order of 2% [15].

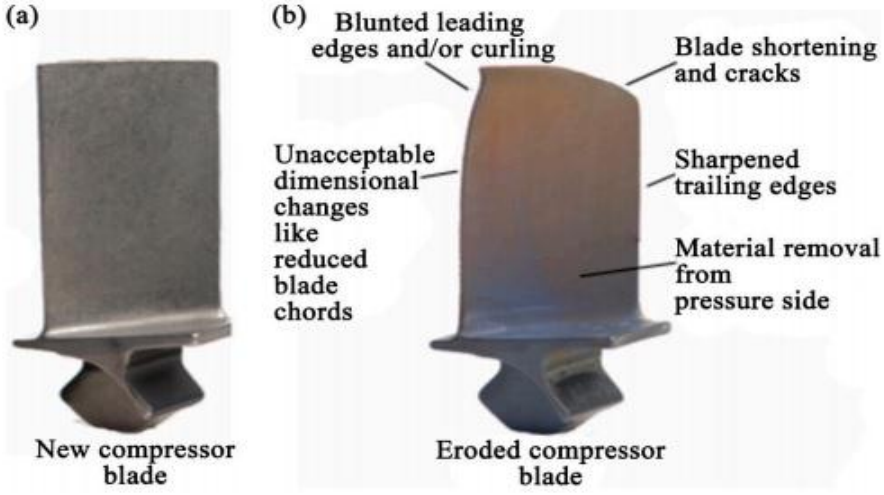

Figure (2.3): Compressor Blades, (a) Demonstrates a New Blade, (b) Shows the Blade After Experiencing Solid Particle Erosion [14]

2.2.4 CORROSION

Material from the gas path components can be removed through chemical reactions with the flow, called corrosion [1]. The products of the reaction may then again adhere to the components, forming a scale [1]. Which leads to a reduction in performance. Figure (2.4) shows an example of corrosion in the turbine blade.

Corrosion can result in the loss of material and an increase in surface roughness. Also, corrosion results in a loss of performance and service life of the component affected [15]. Typically, compressor corrosion results in a reduction in compressor flow capacity and isentropic efficiency, whilst turbine erosion results in an increase in turbine effective area and flow capacity and a reduction in isentropic efficiency [15].

Figure (2.4): Corrosion on the Rise Edge of the Stator Blade of High Pressure Gas Turbine Engine [11]

2.2.5 FOREIGN OR DOMESTIC OBJECT DAMAGE

Damage can be caused by objects getting into the gas turbine. These may be foreign, leading to Foreign Object Damage (FOD), or parts of the engine itself leading to Domestic Object Damage (DOD) [1]. This deteriorates the performance of the engine. The exact damage done depends on the object

and where it hits the internal components [11]. This may lead to such an amount of damage that the operation can no longer continue [1]. Figure (2.5) shows an example of Foreign Object Damage.

Figure (2.5): Foreign Object Damage [11]

2.3 EFFECTS OF COMPONENT DEGRADATION

The changes in the performance of a generic twin-spool turbofan engine due to the degradation of each component will be discussed. The generic layout of the turbofan engine is shown in figure (2.6). The component degradation is modeled by changes in component efficiency and mass flow.

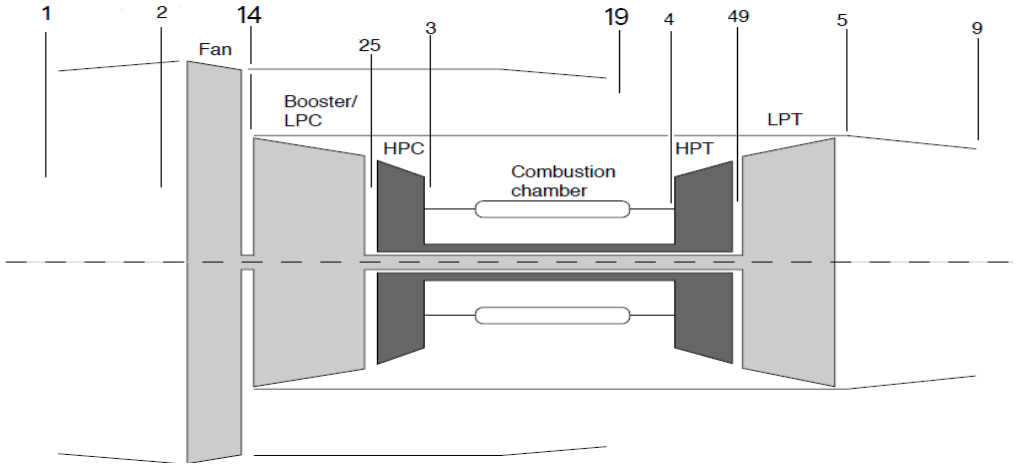

Figure (2.6): Gas Path Geometry of a Twin Spool Turbofan Engine[1]

The effects of degradation are analyzed using simple component maps, compatibility equations, and matching procedures for the off-design performance of a turbofan engine [1].

The performance degradation effects of fouling, erosion, and corrosion are quantified in the table (2.1) [1]. The table shows that the change in component dimensionless mass flow is usually larger than the change in isentropic efficiency. Also, it is found that the changes in turbine mass flow can be both positive and negative. For abrasion, or changes in tip clearances, the same effect is expected, although changes in efficiency are likely larger than with fouling [15].

Table (2.1): Performance Effects Due to Fouling, Erosion, and Corrosion on Component Characteristics [15]

Deterioration	$\Delta\dot{m}_c$	$\Delta\eta_{is}$	$\Delta\dot{m}_c : \Delta\eta_{is}$
Compressor Fouling	↓	↓	± 3-8:1
Turbine Nozzle Guide Vane Fouling	↓	↓	± 2:1
Compressor Erosion	↓	↓	± 2:1
Turbine Erosion	↑	↓	± 2:1
Compressor Corrosion	↓	↓	± 2:1
Turbine Corrosion	↑	↓	± 2:1

2.3.1 LPC Degradation

The first degradation component that will be studied is LPC. The engine is considered to be N1 controlled [1].

LPC Degradation causes a reduction in component corrected mass flow and a reduction of isentropic efficiency, as found in Table (2.1).

The reduction in corrected mass flow through a compressor results in a reduction of the pressure ratio attained by the compressor [15]. This effect can also be seen in figure (2.7). LPC mass flow degradation reduces the pressure ratio of the LPC.

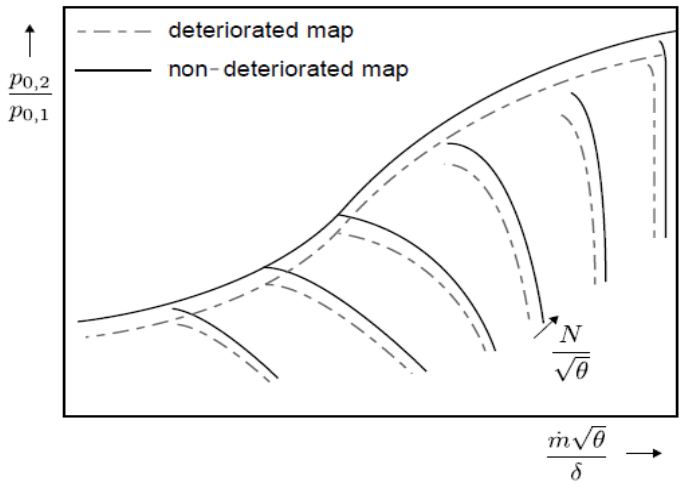

Figure (2.7): Influence of a Reduction in Mass Flow Capacity on a Compressor Map. The Deteriorated Map is Shown with Dashed Lines [1]

After LPC, the flow enters the HPC. Assuming no losses, mass flow compatibility must exit from LPC to HPC [1]. The mass flow compatibility between LPC and HPC is given by equation (2.2). Assuming that the efficiency of the LPC does not change significantly, equation (2.2) dictates that the corrected mass flow entering the HPC will rise [1], which will cause an increase in the HPC pressure ratio and non-dimensional spool speed N2[15]. The temperature ratio and pressure ratio over the LPC compressor are linked by the isentropic relationship, from equation (2.3), the change in temperature ratio is smaller than the change in pressure ratio [1].

$$\frac{\dot{m}\sqrt{T_{025}}}{P_{025}} = \frac{\dot{m}\sqrt{T_{02}}}{P_{02}} \quad \frac{P_{02}}{P_{025}} \quad \sqrt{\frac{T_{025}}{T_{02}}} \qquad \text{(2.2)}$$

$$\frac{T_{025}}{T_{02}} = 1 + \frac{1}{\eta_{is}}\left[\left(\frac{P_{025}}{P_{02}}\right)^{\frac{\gamma-1}{\gamma}} - 1\right] \qquad \text{(2.3)}$$

Between the HPC and HPT, both mass and work compatibility must exist, as they are located on the same shaft [1]. Flow compatibility between the HPC and HPT is given by equation (2.4), and work compatibility is given by equation (2.5), assuming no mass flow changes between both components [1].

$$\frac{\dot{m}\sqrt{T_{04}}}{P_{04}} = \frac{\dot{m}\sqrt{T_{025}}}{P_{025}} \frac{P_{025}}{P_{03}} \frac{P_{03}}{P_{04}} \sqrt{\frac{T_{04}}{T_{025}}} \quad \text{(2.4)}$$

$$\frac{\Delta T_{HPT}}{T_{04}} = \frac{\Delta T_{HPc}}{T_{025}} \frac{T_{025}}{T_{04}} \frac{C_{Pa}}{C_{Pg}\,\eta_m} \quad \text{(2.5)}$$

The ratio P_{03}/P_{04} in equation (2.4) is assumed to be constant. Also, it is assumed that the HPT is choked, which has a constant dimensionless mass flow going through it. By using equation (2.4), it is found that the temperature ratio T_{04}/T_{025} will rise, leading to an increase in EGT and fuel flow. Rewriting equation (2.3) into equation (2.6), shows the relation between the change in pressure ratio and the temperature rise over the HPC [1].

The change in T_{025} will be small [1]. Due to that, the temperature difference over the HPC will increase, which leads to an increased temperature difference over the HPT [1], as shown in equation (2.5). This will lead to a decreased pressure ratio over the HPT, assuming the efficiency does not change [1].

$$\Delta T_{HPc} = T_{03} - T_{025} = \frac{T_{025}}{\eta_{is}} \left[\left(\frac{P_{03}}{P_{025}} \right)^{\frac{\gamma-1}{\gamma}} - 1 \right] \quad \text{(2.6)}$$

The change in LPC efficiency has a small effect on the operation of the engine [15]. This can be explained using equation (2.3), remembering that the pressure ratio over the LPC is small [1]. This will lead to a small change in the temperature ratio.

2.3.2 HPC DEGRADATION

The same equations and principles apply to the LPC. From table (2.1) the same degradation principles apply, with a reduction in both dimensionless mass flow and isentropic efficiency. It must be remembered that the spool speed of the HPC is not controlled actively [1].

The LPC will keep turning at a constant speed, as the assumed engine is N1 controlled. This will result in an increase in pressure ratio over the LPC, which also leads to a slightly increased temperature ratio [1].

As is assumed that the HPT is choked. So due to a decrease in mass flow in HPC, the pressure ratio over the HPC will decrease [15]. Assuming that HPC efficiency does not change much, the temperature ratio over the HPC will decrease slightly [1]. Using equation (2.4) it is then found that the temperature ratio T_{04}/T_{025} must increase, which is caused by an increase in the fuel flow, as does the EGT.

As the work required by the HPC increases, the work delivered by the HPT must rise too [1]. This will increase the temperature difference over the HPT, increasing the temperature ratio. Assuming constant efficiency this will also increase the pressure ratio, decreasing the pressure after the HPT [1].

2.3.3 HPT DEGRADATION

Turbine degradation causes a loss in efficiency and either an increase or decrease in mass flow through the turbine, as is shown in Table (2.1). A turbine transforms the potential energy in the flow into kinetic energy [1]. A less efficient turbine will cause to reduce HPT pressure ratio, spool speed N2, and a reduced temperature ratio through HPT [1]. The HPC is connected to the same shaft with HPT, and will therefore run at a reduced speed. This leads to a reduction of dimensionless mass flow through the HPC

and a decreased pressure ratio generated through the HPC [15]. Investigating equation (2.4), assuming that the HPT is choked, it is found that the ratio T_{04}/T_{025} will increase. This leads to an increase in fuel flow.

Figure (2.8) shows the matching of HPT and LPT [5]. Equation (2.7)

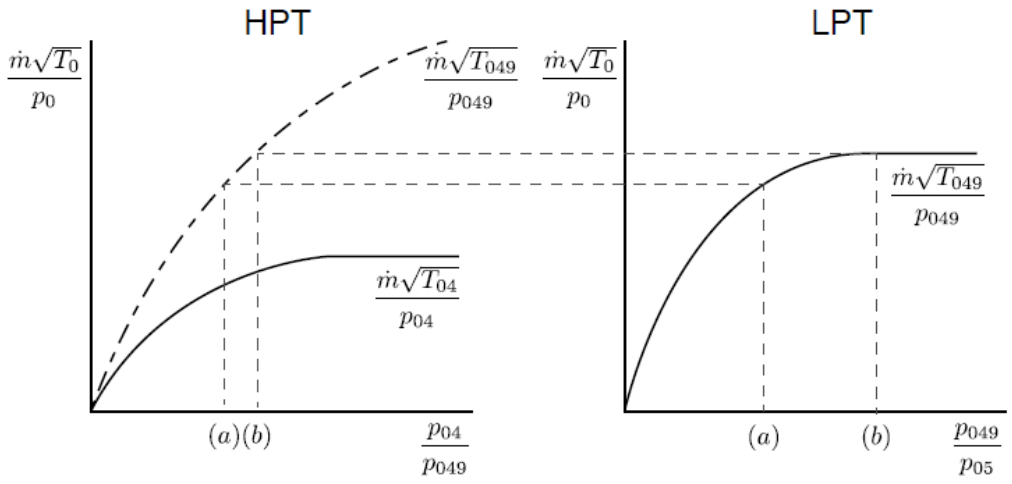

Figure (2.8): Matching of Two Turbines in Series [5]

shows the relation in dimensionless mass flow between the HPT and LPT [5]. Assuming that the efficiency of the HPT does not change much over the operating range, the LPT dimensionless mass flow becomes a function of only the HPT pressure ratio and HPT dimensionless mass flow, as the variation in temperature ratio over the HPT will be small [5]. A choked LPT will therefore dictate the operating point of the HPT [5].

$$\frac{\dot{m}\sqrt{T_{049}}}{P_{049}} = \frac{\dot{m}\sqrt{T_{04}}}{P_{04}} \quad \frac{P_{04}}{P_{049}} \quad \sqrt{\frac{T_{049}}{T_{04}}} \qquad \text{.....(2.7)}$$

From equation (2.6), the change in HPT dimensionless mass flow capacity will be influenced by the presence of the choked LPT [1]. Also, the temperature ratio over HPT will be constant and the dimensionless mass flow through the LPT will be constant, it is found that an increase in dimensionless

mass flow over the HPT will lead to a decreased pressure ratio and vice versa [1].

Assuming that the turbine spool speed does not change due to a change in mass flow (only due to a change in efficiency, which is assumed to be constant) the HPC is only influenced by a change in dimensionless mass flow [1]. At constant spool speed, a reduction in inlet mass flow in HPT will lead to a higher pressure ratio, an increase in mass flow in a decrease in pressure ratio [1].

2.3.4 LPT DEGRADATION

The LPT degrades in the same way as the HPT, with a decrease in efficiency and either a positive or negative change in component dimensionless mass flow.

As it is assumed that the engine is N1 controlled, so the spool speed N1 of the LPT will remain constant [1]. A less efficient LPT will turn at a slower spool speed. To keep the N1 speed constant more energy will have to be added to the flow, increasing the fuel flow and EGT [1].

Changes in mass flow for the LPT are influenced by the presence of the HPT. From equation (2.7), assuming that the HPT is choked and operating at constant efficiency, it is found that with increasing LPT mass flow the HPT pressure ratio will increase and vice versa [1].

Decreasing the dimensionless mass flow through the LPT reducing the HPT spool speed [1]. This is also due to the reduced pressure ratio. The reduced spool speed will decrease the available mass flow through the HPC and reduce the pressure ratio over the HPC [1]. This will reduce the work done in the HPC, allowing the work in the HPT to be reduced too, as well as, the ratio T_{04}/T_{025}, from equations (2.5) and (2.7). The LPC is affected by the LPT

too, an increase in mass flow decreases the pressure ratio over the LPC and vice versa.

2.4 THE GPA CONCEPT

Gas turbine engines are susceptible to various physical problems such as fouling, erosion, corrosion, partially damaged or missing blades, foreign or domestic object damage, tip clearance increase, worn seals, combustor damage, and many others. The behavior of a deteriorated engine depends on the type and severity of the deterioration and the components that are degraded [2].

Component degradation can produce observable changes to measurable performance parameters such as pressure, temperature, and rotational speeds. By analyzing the changes to the measurable performance parameters while taking into account the effects of engine operating conditions and power settings, the presence of component degradation can be detected. This technique is referred to as gas path analysis [2].

Figure (2.9) shows a schematic of the relationship between physical degradation mechanisms, independent component condition parameters, and dependent and observable engine performance parameters. The relation shown in figure (2.9) can be used to monitor the performance of the engine gas path, or for differential GPA [1]. Differential GPA compares a reference gas turbine engine model parameter with measured parameters of the model, such as (engine on-wing, test cell data, etc.). The results must be analyzed by taking the reference engine data into account [1].

It is important to note that not all engine faults can be identified by the use of GPA, such as (vibration, material fractures, fatigue cracks in the rotor disks or blades, etc.) which require other diagnostic methods [1].

GPA gives more insight into the condition of a gas turbine than the traditional method in which only the Exhaust Gas Temperature (EGT) margin is taken into account [2].

GPA can be used to provide more information on the condition of the individual components, rather than on the engine as a whole [2].

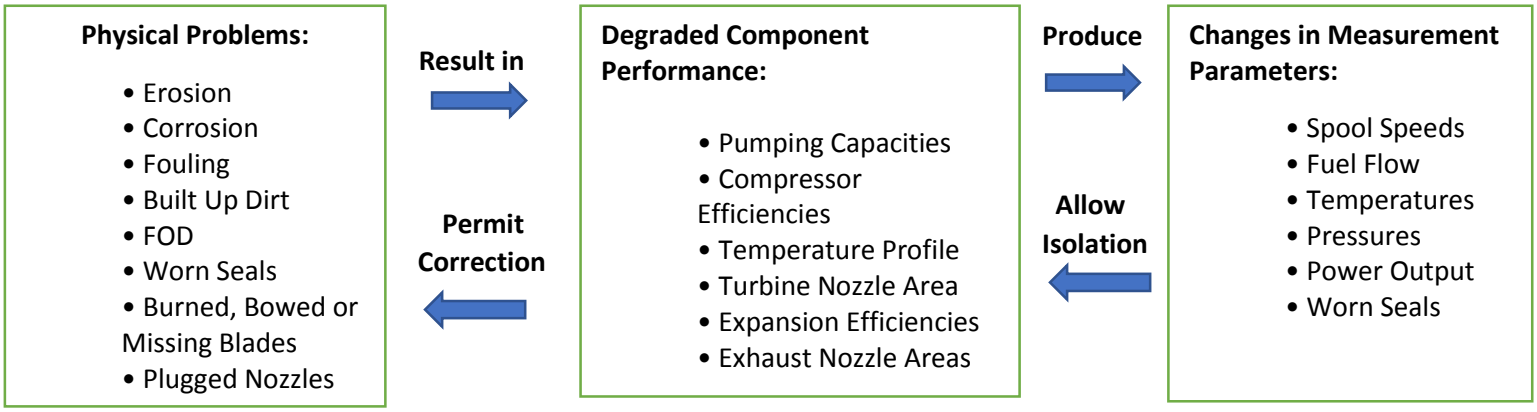

Figure (2.9): Relation Between Physical Degradation Mechanisms, Component Condition Changes, and Observable Engine Performance Parameters [1].

2.5 GAS PATH ANALYSIS METHODS

The different methodologies will be divided into two categories, model-based methods and empirical methods [1]. The model-based methods are based on a thermodynamic model of the gas turbine. Empirical models are based on Artificial Intelligence (AI), numerical methods used to perform GPA [2]

2.5.1 MODEL BASED: LINEAR

Linearized methods are based on the assumption that changes in the measured parameters are small around the steady-state operating point, hence they can be linearized [1]. The linear approximation used is given by equation (3.6) [2].

$$\overline{Z} = H.\overline{X} \quad \text{(2.8)}$$

Here, $\overline{Z}$ is the measurement vector, $\overline{X}$ the performance parameter vector, and **H** is the Influence-Coefficient Matrix (ICM). Multiplying both sides of equation (2.8) with H^{-1} gives equation (2.9).

$$\overline{X} = H^{-1}.\overline{Z} \quad \text{(2.9)}$$

The inverse of the ICM is called the Fault-Correlation Matrix (FCM). Equations (2.8) and (2.9) can also be written as equations (2.10) and (2.11) relating the differences to each other [2].

$$\Delta\overline{Z} = H.\Delta\overline{X} \quad \text{(2.10)}$$

$$\Delta\overline{X} = H^{-1}.\Delta\,\overline{Z} \quad \text{(2.11)}$$

The linear method is a simple and fast technique [2]. The linear method drawbacks can be found when investigating equations (2.8) and (2.9). The conversion from ICM to FCM requires that the ICM is invertible, and the ICM must be a square matrix, requiring equal measurements and performance parameters [2]. This may not always be possible in an actual gas turbine. The Accuracy of the method depends on the accuracy of the ICM [2].

The linearity assumption is only acceptable in a small region around the steady state point [1]. This is shown visually in figure (2.10) [1].

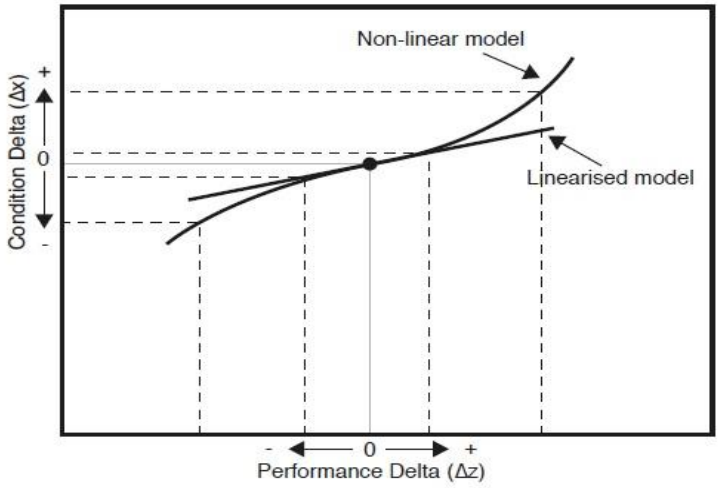

Figure (2.10): Accuracy Differences Between a Linear and Non-Linear Model [1]

2.5.2 MODEL BASED: NON-LINEAR

The performance of gas turbines cannot be described linearly without making use of large and not fully valid assumptions [1]. GPA non-linear methods have been divided into two methods [1]. Both methods rely on optimization in order to find the condition of the gas turbine [1].

The first method relies on the Newton-Raphson root-finding method [1]. The linear method is applied repeatedly, converging towards the actual condition of the gas turbine while taking the nonlinearity into account. This method is also described by Escher and used in the Pythia software package [15].

The second modeling technique is Adaptive Modelling (AM), first described by Stamatis et. Al [16]. This method relies on adapting the engine model to accurately describe the measured performance [1]. The model is adapted by changing the compressor and turbine maps [1]. The changes made to the maps correspond to the differences in component conditions between the measured and baseline engine. Isentropic efficiency and corrected mass

flow in a component map, are needed to fully describe the operating points of the engine component.

Adaption of the model is done numerically. Adaption can be done either internally or externally [16]. Internal adaption can be done if the AM equations are added directly into the simulation model. External optimization puts the AM equations outside of the model, externally iterating the simulation procedure [16]. The difference is represented visually in figure (3.3) [7].

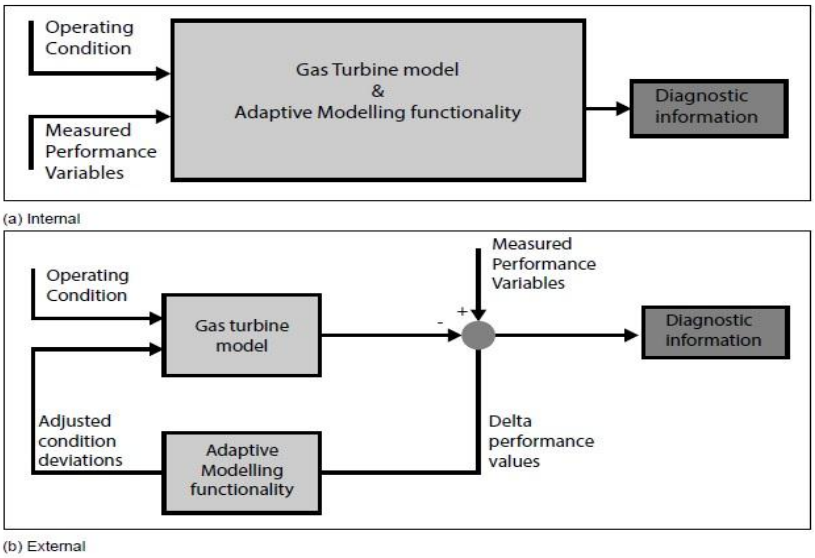

Figure (2.11): Internal and External AM Strategies [7]

2.5.3 EMPIRICAL: ARTIFICIAL NEURAL NETWORKS

Empirical methods have been developed to overcome the inherent problems of model-based methods, convergence issues, and the inability to deal with measurement uncertainty [2]. Furthermore, they are developed to overcome the need for large amounts of measurements and sensors, and the need for linearization altogether [1].

The empirical methods are Artificial Neural Networks (ANNs). As the name already suggests, ANN aims to mimic the biological brain. Consisting of a series of parallel distributed processors it has the ability to store knowledge as experience and the ability to apply this knowledge [1].

ANN needs to be trained to produce the useful output [2]. ANNs have the ability to learn and generalize [2]. Due to this property, they are able to deal with cases not exactly available in the set of training data. This allows them to deal with sensor bias and noise. Although ANN is treated here as one class of methods, many different kinds of ANNs can be developed [1].
ANNs also have their disadvantages. Although a trained ANN performs quickly, training times are long and require vast data sets [2]. Retraining might be required when operating conditions change [1]. Finally, ANNs are unable to perform well outside of the scopes of their training data set [2].

2.5.4 EMPIRICAL: GENETIC ALGORITHMS

Genetic algorithms (GAs) are a type of optimization algorithm. GAs are based on evolutionary principles to find the optimal solution to a problem [2]. Starting with a range of solutions the first step is to apply a selection procedure to find the solutions that will advance to the next generation. Crossover is then applied to these solutions, to form new solutions consisting of the combined information from the two parent solutions. Finally, a mutation step is added to introduce new or lost information to the solution set [1].

Analysis using GAs is highly time-consuming, limiting the practical use of GAs. Due to the high complexity of modern gas turbines, many faults can occur, increasing the degrees of freedom for the analysis and decreasing the effectivity of GAs [2].

2.5.5 EMPIRICAL: EXPERT SYSTEMS

An ES consists of a knowledge base and an interference engine [2]. Information is stored inside the knowledge base, which is accessed by the interference engine, using a range of different logics [2]. This way the system mimics the way in which a human expert would work [2].

The single largest advantage of using an ES for GPA is the ability of an ES to combine different diagnostic techniques [2]. This would for example allow for the possibility of combining GPA with vibrational analysis.

ESs like ANNs require vast datasets to perform properly, which is a disadvantage of the method [2]. The response of the system might also change when new information is added to the knowledge base, as the system tries to incorporate this information into the analysis. As the response to previously analyzed situations can also change, the system has to be revalidated in order to be used after the information has been added [2].

CHAPTER 3

DESIGN POINT MODELLING

This chapter is the starting point for the development of the GSP model representing the CF6-80C2, it includes the assumptions made about the engine model. With these steps out of the way, a start can be made with modeling the CF6-80C2.

3.1 ASSUMPTIONS

As a model is a simplified depiction of the actual engine, more assumptions are introduced when creating the model. The assumptions are made due to a lack of data about detailed information about the engine. The information about the engine is readily available about some performance of the engine in operation and about mechanical details and repairs. However, it is unknown what each system does exactly at each operating condition. This information gap creates an additional challenge when creating the model, leading to additional assumptions to be made.

The design point of a model can be different from the actual design point of the engine [1]. It is then possible to design the individual components of a gas turbine so that the complete unit will give the required performance when running at the design point; that is when it is running at the particular speed, pressure ratio, and mass flow for which the components were designed [5].

In previous studies at KLM ES take-off power at International Standard Atmosphere (ISA), sea level conditions have been chosen as the design point for the model [2]. This point was chosen as it is the most demanding tested power setting in the KLM ES test cell [1].

Take-off has been chosen as the design power setting for the engine model. The take-off power setting as tested in the test cell is the maximum amount of thrust that the engine can deliver. It is expected that performance issues with a specific engine are clearest at this power setting [1]. Designing the model at this point is then expected to give the most accurate analysis results [1]. Some assumptions will be taken as the following:

- **Variable Geometry**: CF6-80C2 is outfitted with several variable geometry systems, such as VSVs and VBVs. During operation these influence how the engine performs. It is unknown what schedules these systems operate, so that, the variable geometries will not be modeled, and are assumed to be nonexistent in the model.
- **Bleed Air and Cooling Flows**: Besides the thrust of CF6-80C2, the air is also used to pressurize parts of the engine, for de-icing purposes, cooling, and other purposes. Only the maximum amounts of air are known for extraction for booster anti-icing are available, so that, Bleed air and cooling flows assumed to be nonexistent in the model.
- **Engine Rating**: The CF6-80C2 is available with different ratings, each having its own performance. The rating is changed in the Engine Control Unit using a rating plug, engine performance differs between the different ratings. This model will present the Take-off of the CF6-80C2 model.

3.2 ACQUIRED DATA

The following data shown in table (5.1), are shown the GPA results of the test cell at a takeoff power setting of engine CF6-80C2 taken from [2], which will be the reference data for the engine model of CF6-80C2, the locations of the gas path measurements are shown in figure (2.6).

Table (3.1): Design Point Input Data Parameters (Reference Data) [2]

Parameter	**Description**	**Value**	**Unit**
N1	Fan Speed	3525	rpm
N2	Core Speed	10537	rpm
FN	Net Thrust	255.56	KN
W_f	Fuel Flow	2.69	kg/s
Tt49 (EGT)	HPT Outlet Temperature	1123	K
Tt2	Fan Inlet Temperature	289	K
Tt25	HPC Inlet Temperature	389	K
Tt3	HPC Outlet Temperature	838	K
Pt2	Fan Inlet Pressure	1.011	Bar
Pt25	HPC Inlet Pressure	2.593	Bar
Ps3	HPC Outlet Static Pressure	32.063	Bar
Pt49	HPT Outlet Pressure	7.612	Bar
RH	Relative Humidity	78.93	%

The above data shown in table (3.1), is not enough to build the design point model of the engine, which leads to an increase in the assumptions and prediction of the remaining data. The measured parameters located in the table

(3.1) are referred to the locations of the gas path measurements shown in figures (2.6) and (3.1).

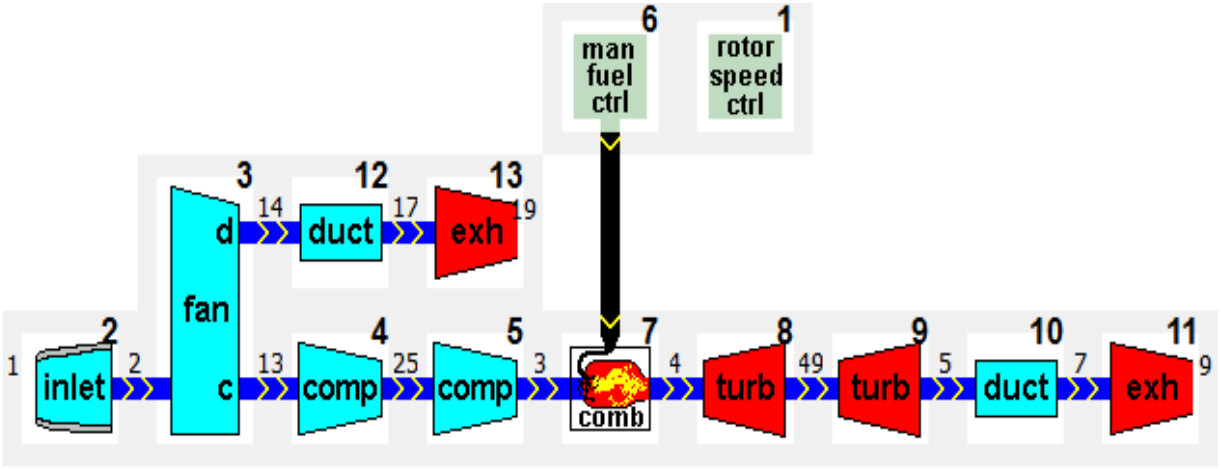

Figure (3.1): Layout of the CF6-80C2 Model in GSP

By using the generic components available in GSP, the CF-80C2 model has been built, and the layout of the model is shown in figure (3.1). Important to note is the presence of a compressor component for the booster in figure (3.1), which is different from figure (1.3). unfortunately, no performance parameters measurements are taken between the fan core and booster inlet in reference data shown in table (3.1). Previous researchers such as ML Verbist [2], he has modeled them (Fan core + Booster) as a single component in the GSP model, which require him to do a new component map that combined the performance characteristics of both components together, which is really long work. In this thesis and to simplify this problem, the GSP generic components maps are used for each component with isolation of the booster and fan core, these generic component maps in the GSP are simple to scale to the model design point.

Because of the limited measured performance parameters shown in table (3.1), component conditions can't be determined for all turbomachinery

components, and special adaptations to the model were necessary to use the available measured performance data. The generic modeling capability of GSP is particularly advantageous to accommodate the required adaptations. The steps taken to determine the design point properties are stated below [1].

- Adapt the ambient conditions to match the test cell conditions.
- Set the fuel flow to the combustion chamber to what is measured in the test cell.
- Set the overall mass flow: **assumed because it isn't available.**
- Adapt the LPC pressure ratio to match TT25.
- Adapt the HPC pressure ratio to match PS3: **The measured HPC outlet pressure is a static measurement. In order to compute the total pressure, the flow path area of the tube running from the combustor diffuser to the Electronic Engine Control (EEC) is needed, GE, unfortunately, does not disclose the exact flow areas inside the engine. As the basic operation of an axial flow compressor, the working fluid is initially accelerated by the rotor blades, and then decelerated in the stator blade passages wherein the kinetic energy transferred in the rotor is converted to static pressure [5]. in this case it is considered to assume that PS3 ≈ Pt3.**
- Adapt the HPC efficiency to match TT3.
- Adapt the bypass ratio (BPR) to match TT49.
- Adapt the LPC bypass pressure ratio to match the measured thrust.

Following these steps, an iterative process has been done by GSP, which if done by hand, can be time-consuming. GSP components allow the user to fix output parameters and set the component properties free to be adapted during design point calculations.

Isentropic efficiencies of engine components, mechanical efficiency of both shafts, and combustion efficiency have to be assumed as well, according to values found in [1], and by adapting the model as the above steps. The design point isentropic efficiencies of the CF6-80C2 model are presented in table (3.2).

Table (3.2): Efficiencies of CF6-80C2 Design Point Model Values

Variable	Description	Value
$\eta_{is,inlet}$	Inlet Isentropic Efficiency	1.000
$\eta_{is,fan\ core}$	Fan Core Isentropic Efficiency	0.93
$\eta_{is,fan\ duct}$	Fan Duct Isentropic Efficiency	0.93
$\eta_{is,LPC}$	LPC (Booster) Isentropic Efficiency	0.868
$\eta_{is,HPC}$	HPC Isentropic Efficiency	0.853
$\eta_{is,HPT}$	HPT Isentropic Efficiency	0.9146
$\eta_{is,LPT}$	LPT Isentropic Efficiency	0.9
$\eta_{j_{bypass}}$	Bypass Nozzle Efficiency	0.9719
$\eta_{j_{core}}$	Core Nozzle Efficiency	0.972
η_m	Mechanical Efficiency	0.990
η_{cc}	Combustion Efficiency	0.995

With the necessary assumptions made the model as shown in figure (3.1) can be finished. Following the steps above, the model design point has been finished at a takeoff power setting. The input data for the model is given in table (3.3). In the table (3.3), the ambient pressure and temperature are considered as the reference data in the table (3.1), and the mass flow rate is assumed based on some references such as [20]. N1 speed of 107.47% has

been taken from [2], and the N2 speed of 107.22 from [19]. Beta values or parameters are ranging between 0 to 1, the beta parameter is used to avoid numerical convergence problems during iterations towards the operating point solutions in off-design, these values are assumed in each component to control the design point location in the components map [3]. The adapted model parameters are shown in table (3.4), and the design point model parameters are in table (3.5).

Table (3.3): Design Point Model Input Parameters

Parameter	**Description**	**Unit**	**Value**
Ta	Ambient Temperature	k	289
Pa	Ambient Pressure	bar	1.011
M	Mach Number	----	0
RHUM	Relative Humidity	%	78.93
WF	Fuel Flow	kg/s	2.69
WA2	Total Engine Mass Flow	kg/s	808
N1	Fan Speed	%	107.47
N1	Fan Speed	rpm	3525
N2	Core Speed	%	107.22
N2	Core Speed	rpm	10537
$\beta\ Fan\ Core$	Fan Core Map Design Beta Value	-----	0.571429
$\beta\ Fan\ Duct$	Fan Duct Map Design Beta Value	----	0.571429
$\beta\ LPC$	LPC Map Design Beta Value	----	0.571429
$\beta\ HPC$	HPC Map Design Beta Value	----	0.60979
$\beta\ HPT$	HPT Map Design Beta Value	----	0.864906
$\beta\ LPT$	LPT Map Design Beta Value	----	0.700

Table (3.4): Design Point Model Adapted Parameters

Parameter	Description	Unit	Value
OPR	Overall Pressure Ratio	----	31.65
$PR_{fan\ core}$	Fan Core Pressure Ratio	----	1.5
$PR_{fan\ duct}(FPR)$	Fan Duct Pressure Ratio	----	1.521
PR_{LPC}	LPC Pressure Ratio (Booster)	----	1.71
PR_{Hpc}	HPC Pressure Ratio	----	12.34
BPR	Bypass Ratio	----	5.01
Tt4 (TIT)	HPT Total Inlet Temperature	k	1504.53

Table (3.4) shows how the model has been adapted by the procedure as described above to match the test cell measurements. The biggest pressure increase is reached in the HPC, with a slight increase caused by the booster. The overall pressure ratio is almost equal to the value mentioned in GE promotional material [8].

Table (3.5): Model Output Parameters and Reference Data Comparison

Parameter	Description (Unit)	GSP	Reference	Difference %
Tt25	HPC Total Inlet Temperature (k)	389.04	389	0.0004
Pt25	HPC Total Inlet Pressure (Bar)	2.59321	2.593	0
Tt3	HPC Total outlet Temperature (k)	838.28	838	0.0028
Tt49 (EGT)	HPT Total Outlet Temperature (k)	1123.79	1123	0.0079
Pt49	HPT Total Outlet Pressure (Bar)	7.61236	7.612	0
FN	Thrust (KN)	255.561	255.56	0.1%

The results in table (3.5) show that the values as computed by the GSP model represent very well results for the design point calculation. There is an agreement between GSP model results, and reference values, as shown in the table (3.5). The biggest deviation is in the computed FN value, with a difference between the values of 0.1%, which is a very small.

In this chapter the design point model of the CF6-80C2 has been fixed, providing a reference point for the off-design calculations which will follow next. Due to a reduced number of measurements, several assumptions have been made on the performance of engine components. The design point performance for a turbofan engine will be presented in Appendix C.

CHAPTER 4

OFF-DESIGN MODELLING

It was indicated in Chapter 1 that the off-design simulation in GSP depends on component maps so that they can accurately represent the performance of the real engine components. For the purposes of design modeling, the model needs merely match the measured parameters. Outside of the OEM, the component maps defining the performance of the CF6-80C2 are not accessible, necessitating the use of publically accessible maps.

4.1 OFF-DESIGN DESCRIPTION

The nonlinear system equations relating to the laws of mass and energy conservation form the basis of the off-design simulation model. The number of equations in the set depends on the number of components in the modeled engine [7].

By resolving the set of system equations, GSP determines the new steady-state operating point (transient performance calculations are also feasible). Satisfying the equation set warrants a physically sound solution e.g. that the air mass flow going through the compressor is equal to the air mass flow going through the subsequent turbine. And, power equilibrium between the compressor and the turbine on the same shaft [7].

In order to satisfy the set of system equations (all equal to zero), an equal number of engine performance variables (states) S has to be determined, such as fuel mass flow, compressor pressure ratio, turbine pressure ratio,

corrected mass flow, and rotor speed(s). Equation (4.1) shows the implicit form of a set of (n) error equations [7].

$$\begin{aligned} f_1(S_1,P,U) &+ \cdots + f_1(S_n,P,U) = 0 \\ &\vdots \qquad\qquad\quad \vdots \quad\ \vdots \\ f_n(S_1,P,U) &+ \ldots + f_n(S_n,P,U) = 0 \end{aligned} \qquad \ldots\ldots\ldots\ldots\ldots\ldots (4.1)$$

The equations in the set are a function of

- Si: n independent state variables
- P: a vector consisting of gas path performance variables
- U: a vector containing power control settings and ambient conditions

The simulated performance is dependent on the operating conditions imposed on the model. Moreover, the performance map used in each sub-model plays an important role. Like in the real engine, the performance of the components affects to a large extent the power equilibrium that is obtained between the compressors and turbines in the gas generator. In order to solve the system an iterative calculation is performed using the Newton-Raphson method [7].

For solving the non-linear differential equations (NDEs) GSP defines the operating point by states (or 'free states') in a state vector. Using the appropriate aero thermodynamics equations, maps, and other relations, all engine parameters can be directly derived from the states. As such, the states represent the unknowns in the NDE set to solve for [3].

The NDEs are depending on the state vector and each NDEs has an error variable representing the deviation from a valid solution. The GSP solver iterates towards the solution where all errors (i.e. the error vector) are zero (within the user-specified tolerance) [3].

For a simple turbojet model, for example, there are 4 states and 4 errors. For more complex models such as turbofan models with several schedulers, the number of states and equations may easily rise up to 20 or more [3].

Although most states and errors are set up automatically by GSP, the user can have control over states and errors using component model options. The current maximum amount of model state variables is set to 50 [3].

In this thesis, facilities of GSP will be used, which use the publicly available maps (Compressors and Turbine maps), GSP scales these maps to the aimed model characteristics. So GSP automatically scales the component maps based on the computed design point, which has been established in chapter 5 and the location of the design point on the map. The location on the map can be set by the user, by fixing the design point corrected spool speed and beta line. Due to this mechanism, the publicly available maps can be scaled to fit the CF6-80C2 engine model design point.

4.2 CF6-80C2 ENGINE COMPONENT CHARACTERISTICS (MAPS)

In this chapter, the off-design of the engine model CF6-80C2 will be simulated in GSP by changing the conditions that were used in the design point model. Cruising Speed at Altitude 10000m and 0.8 Mach Number were input to the engine model.

In GSP, the map files consist of tables with corrected mass flow, efficiency, and pressure ratio as a function of corrected normalized rotational speed and beta [3]. The map operating point corresponding to the design operating point is specified using the map design rotational speed and beta values [3]. The design point can be seen inside the graph (component map).

In the map graph also the beta lines can be shown after activating the appropriate item in the Options menu.

The compressor Maps (Fan Core, Fan Duct (Bypass), LPC (Booster), and HPC) are shown in figures (4.1), (4.2), (4.3), and (4.4) respectively. it should be noted that the dashed line behind the design point in the map represents the steady-state case of the cruising by 0.8 Mach number and 10000m altitude.

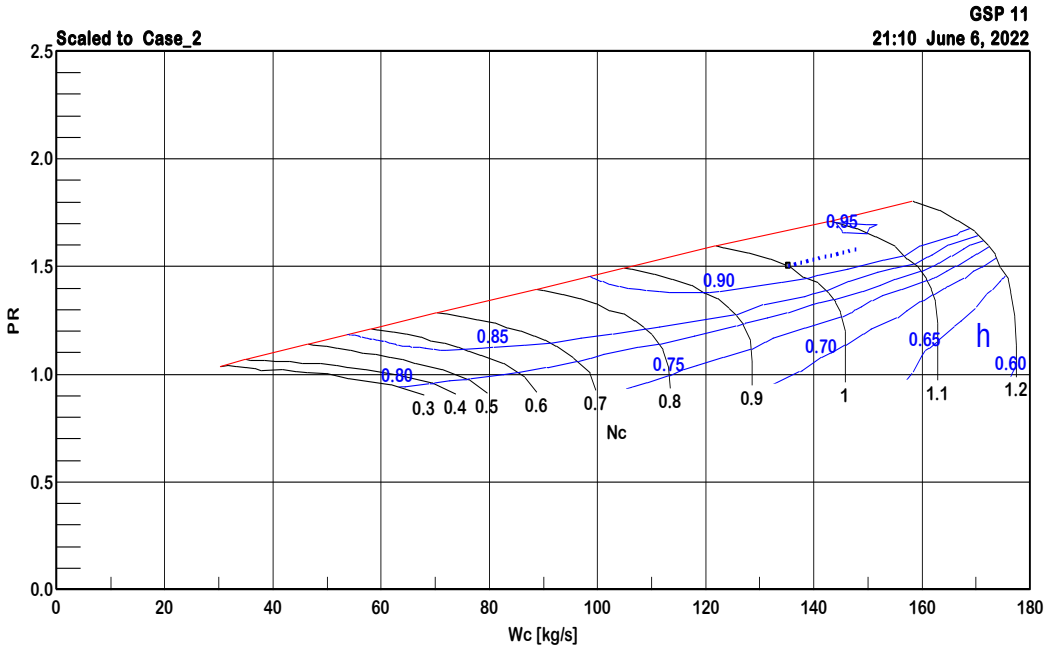

Figure (4.1): Fan Core Map Characteristics

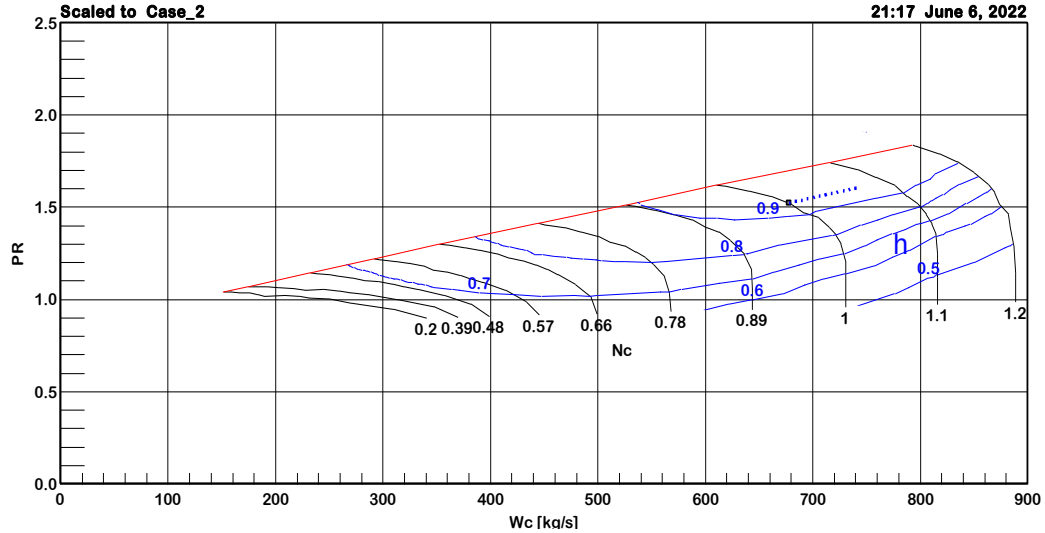

Figure (4.2): Fan Duct Map Characteristics

The Turbines Maps (HPT and LPT) are shown in figures (4.5), and (4.6) respectively.

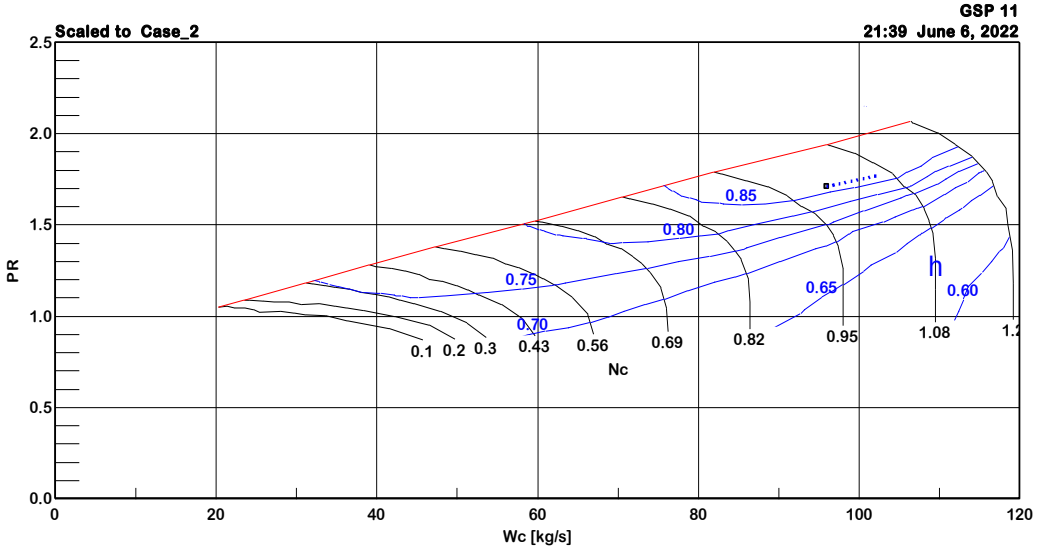

Figure (4.3): LPC (Booster) Map Characteristics

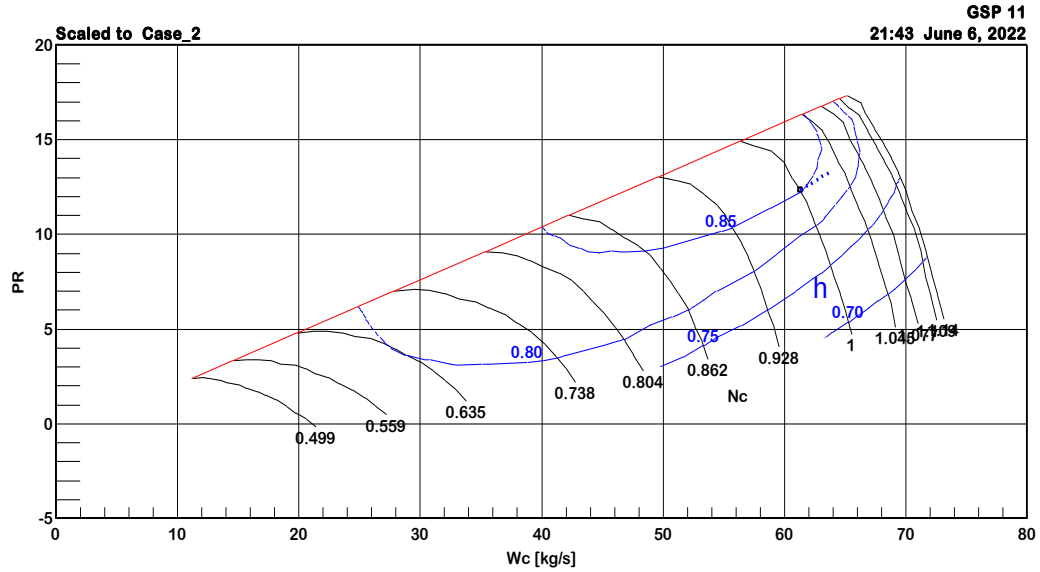

Figure (4.4): HPC Map Characteristics

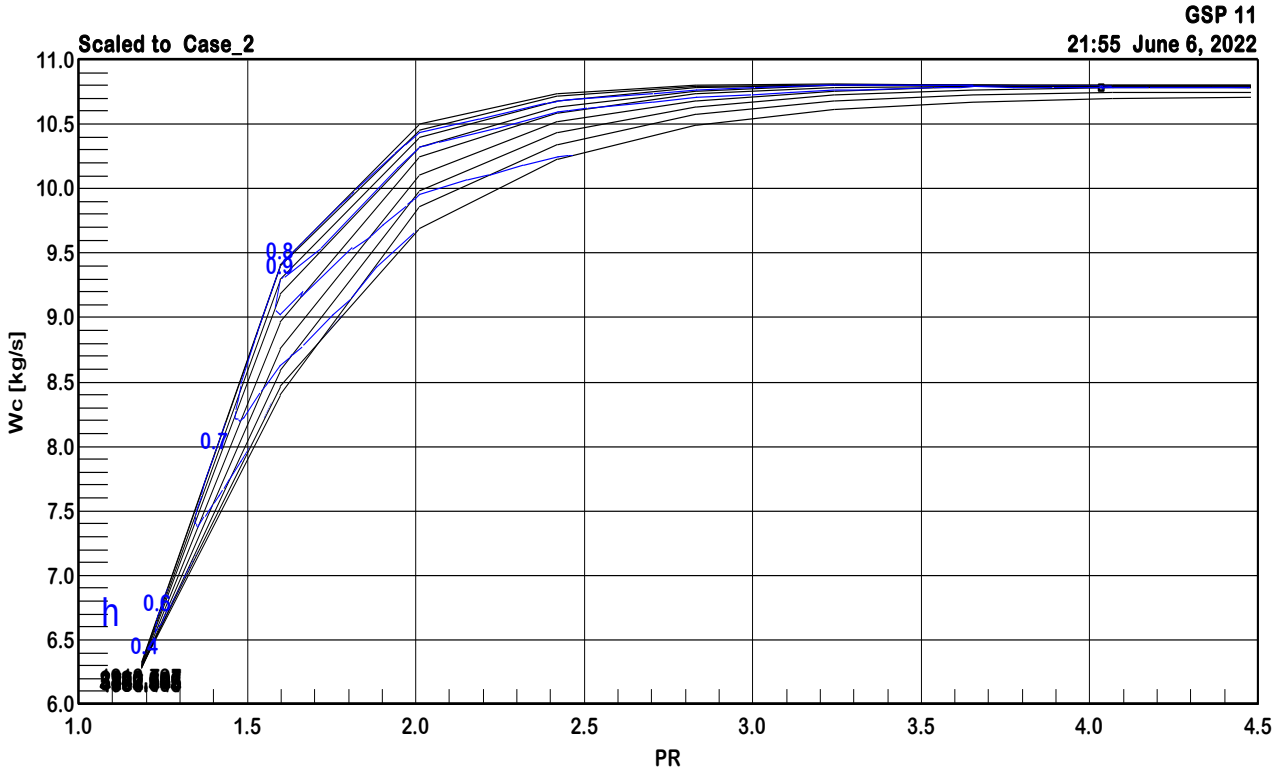

Figure (4.5): HPT Map Characteristics

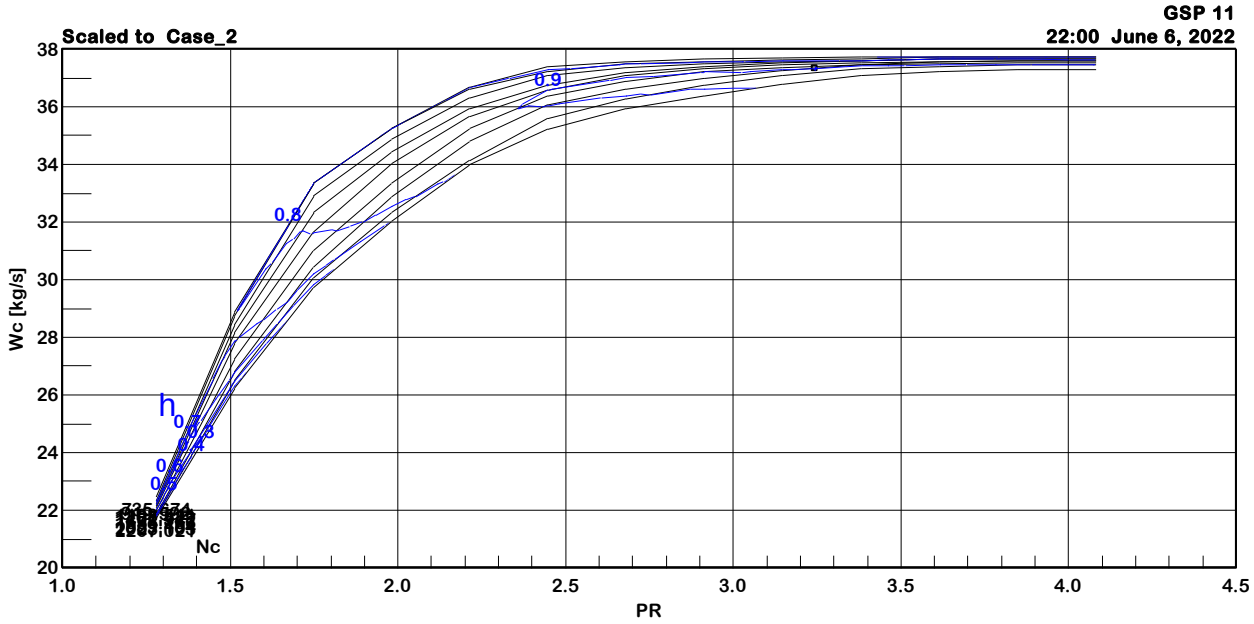

Figure (4.6): LPT Map Characteristics

Despite the unavailability of the original component maps, the off-design performance of the CF6-80C2 can be simulated using the tuned publicly available maps. The CF6-80C2 LPC (core and bypass), HPC, HPT, and LPT maps have been scaled to match the design point parameters.

As mentioned above that the off-design model is simulated at a cruising speed of 0.8 Mach number and altitude of 10000m with adapting the ambient conditions automatically in GSP. it is must be noted that most of the output parameters are changed due to changes in the flight ambient conditions and speed, leads to changes in the air mass flow, fuel consumption, thrust, TIT, etc. that are clear in the component maps. The compressors (Fan Core, Fan Duct, LPC (booster), and HPC) are at a steady state, far from the surge line, and the turbines (HPT, LPT) are chocked, these conditions are very important when deteriorations simulations will be applied and analyzed to the CF6-80C2 engine model.

CHAPTER 5

APPLING SIMULATION OF DETERIORATIONS TO THE ENGINE MODEL CF6-80C2

When applying the design point of the model in chapter 3, some assumptions had to be made, due to a lack of information in the model. In modern studies in some Engine Services such as KLM ES, with their facilities (Engine test cell, detailed information about many aero engines, etc.) they could study, and analyze the performance and the deteriorations of the engines, by using Adaptive Modelling (AM), or other techniques as it mentioned in chapter 3 and comparing the results with flight data (Engine On-Wing) according to the facilities such as engine test cell, available engine on-wing flight data.

Adaptive modeling techniques as shown in chapter 3, rely on adapting the engine model deteriorations accurately, is to specify the associated effects on component performance degradation in the model. The model is adapted by changing the compressor and turbine maps. Adaption of the model is done numerically and then programmed by one of the programming languages and added to the GSP AS AM tool, which is not publicly available and is very expensive to buy. The GSP team gave me a license key to use some facilities of the program, without AM tool, which is really hard to program and time consumable. So based on my supervisor's advice, he instructed me to simulate the deteriorations of the engine model by using some of the assumptions, according to previous references such as reference [1], then apply it to the

GSP, after that, the results will be shown on the graphs, and will be discussed as well. The different types of the deteriorations simulated are shown in table (5.1).

5.1 METHODOLOGY

Various gas turbine component deteriorations were discussed in chapter 2, which includes compressor fouling, Turbine corrosion, erosion, and other physical problems that may occur on gas turbine engines, also their implication on gas path parameters is known. It was discussed that the measured parameters of components have non-linear relation with their respective health parameters (as known in components maps). In this chapter, the deteriorations of health parameters are introduced to the CF6-80C2 engine model in GSP, and their respective deviations in measured parameters as shown in table (5.1) are noted. Various intensity of deterioration is simulated in GSP and their analysis will be done too.

The deterioration study can be done using the GSP deterioration tool, where the user can specify the percentage of deviation in the health parameters (only in compressors and turbines, no deterioration simulated will be done in the combustion chamber).

The deteriorations can happen in a single component (compressor or turbine), and also in multiple components at the same time (compressors and turbines), so that, using GSP deteriorations to the mass flow, and efficiency will be applied to the engine core (LPC (booster), HPC, HPT, and LPT), the fan core and duct will not be simulated for the deterioration.

With the assumptions shown in table (5.1), seven different cases have been defined. The different cases have been divided into two categories as

shown in table (5.1). The first category (I. Basics) contains four cases, which have the purpose of investigating the ability of the model to detect the different types of single-component degradation. Note that for the turbines an increase in mass flow capacity is simulated. The next category is (II. Core+) investigates the ability of the model to analyze the core engine multiple components deteriorations, which assumes an increase in turbine mass flow capacity.

Table (5.1): Simulated Deterioration Cases on CF6-80C2 Engine

Case		LPC Core		HPC		HPT		LPT	
		$\Delta\eta$	ΔW_C	$\Delta\eta$	ΔW_C	$\Delta\eta$	ΔW_C	$\Delta\eta$	ΔWC
I. Basics	1	-1	-3						
	2			-1	-3				
	3					-1	+2		
	4							-1	+2
II. Core +	5	-1	-3	-1	-3				
	6					-1	+2	-1	+2
	7	-1	-3	-1	-3	-1	+2	-1	+2

5.2 RESULTS

Results of the analysis with simulated deterioration are located in figures (5.1) to (5.7). In the figures, the simulated amount of deteriorations and their degradations on the reference parameters shown in table (5.1) are plotted. it should be noted the component of (rotor speed ctrl) in figure (3.1) is Used to specify the rotor speed of a selected shaft (N1 or N2). This component adds an error equation to the model (spool speed, requested spool

speed) and thus requires setting an extra state to the model (e.g. fuel flow to free state) [3]. Fuel flow can be specified as a 'free state' in order to calculate an off-design operating point, with (instead of user-specified fuel flow Wf, combustor exit temp (TIT). or fuel-air ratio) [3]. Using the Fuel flow as a free-state model option always requires the setting of another component's option to provide an extra error variable to maintain an equal number of model states and error variables. Also, the compressors (LPC and HPC) and turbines (HPT and LPT) have been chosen as a free state, to avoid unbalance of the number of statuses and the number of variables. In this thesis, the rotor speed N1 will be fixed in the off-design model calculations, as it considered to be N1 controlled the engine.

5.2.1 RESULTS CATEGORY (I. BASICS)

Case1: LPC deteriorated presented a reduction in its corrected mass flow rate ($LPCW_C$) and isentropic efficiency ($LPC\eta$) as shown in table (5.1), which represent the case of LPC fouling. The engine on which the effect of deterioration is considered to be N1 controlled, so, the reduction in $LPCW_C$ results in a reduction in LPCPR (booster) as shown in figure (5.1a), mass flow compatibility must exist between LPC and HP, leads to increase corrected mass flow rate entering the HPC, the increased in $HPCW_C$ caused an increase in HPCPR and increased the shaft speed N2 about 0.7%, leads to a slight increase in temperature ratio and difference over the HPC. Between the HPC and HPT, both mass and work compatibility must exist, as they are located on the same shaft. As it is assumed that HPT is chocked, the dimensionless mass flow is assumed to be constant through it, so that, the temperature difference over the HPC increased, which leads to an increase in the temperature difference over the HPT, which leads to a decrease the pressure ratio over the

HPT, Using equation (2.4) it is found that the temperature ratio Tt4/Tt25 rose as may note that from figure (5.1), due to this the EGT (Tt_4) and fuel flow increased about 1.24% and 0.51% respectively, resulting in a reduction in the thrust FN of about 0.26% as may note in figure (5.1).

The change in LPCη has a small effect on the operation of the engine as explained in equation (2.3), as well as the LPCPR is small, which leads to a small change in temperature ratio. The changes in component's temperature ratios due to the decrease in LPCWC are presented in figure (5.1b).

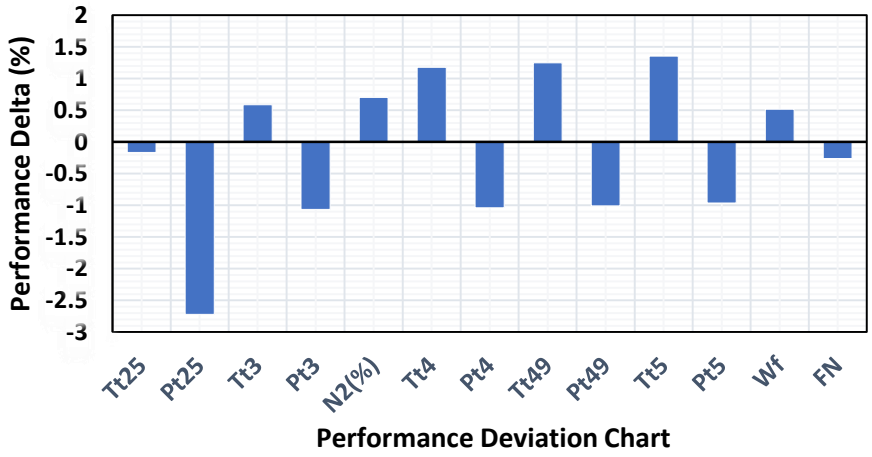

Figure (5.1): GPA of CF6-80C2 Engine GSP Model, Deteriorations Parameters Results for Case1

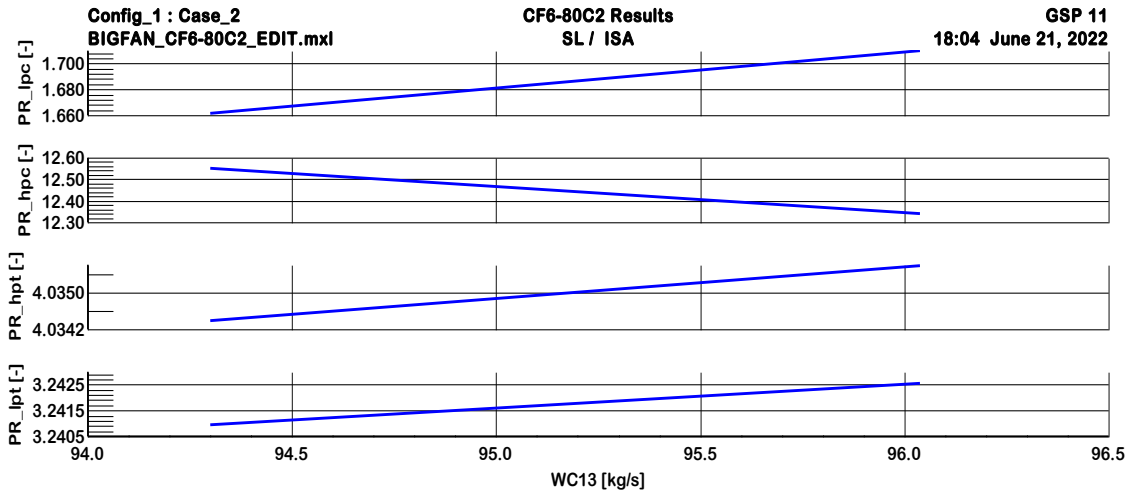

Figure (5.1a): GPA of CF6-80C2 Engine GSP Model, Changes of W13 with Engine Core Components Pressure Ratios for Case1

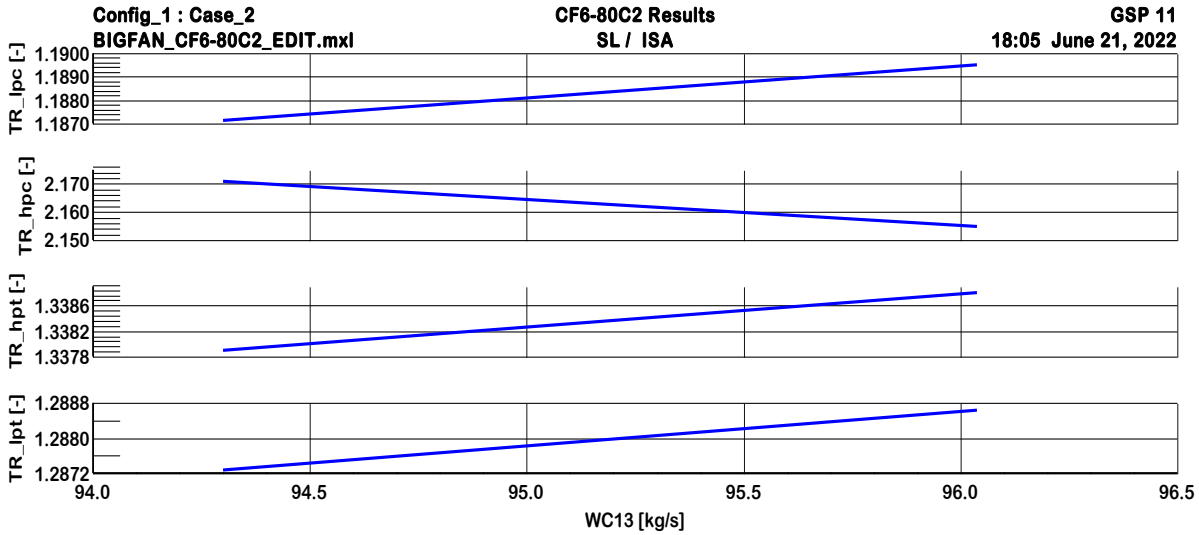

Figure (5.1b): GPA of CF6-80C2 Engine GSP Model, Changes of W2 with Engine Core Components Temperature Ratios for Case1

Case2: HPC is degraded introduced by decreasing in corrected mass flow rate ($HPCW_C$) and isentropic efficiency (HPCη), representing the case of HPC fouling. The LPC will keep turning at a constant speed, as it is assumed that the engine is N1 controlled, this leads to an increase in pressure

ratio and a slight increase in temperature ratio over the LPC as shown in figures (5.2), (5.2a), and (5.2b) respectively. It is again assumed that the HPT is choked, due to decreasing in $HPCW_C$, the HPCPR decreased, HPC temperature ratio and difference slightly increased due to the decrease HPCη, as may note that by investigation equation (2.3).

As could be noted from figure (5.2) Tt_4/Tt_{25} increased, which caused an increase in fuel flow by about 1.18%, as the EGT increased by about 1.42%. As the work required by the HPC increases, the work delivered by the HPT must rise too as they are located on the same shaft, this leads to an increase in the temperature difference over the HPT, increasing the temperature ratio, and also causing to increase the shaft speed N2 about 0.39%.

Due to decreasing in HPCη the pressure ratio over HPT decreased, with decreasing in the pressure after HPT.

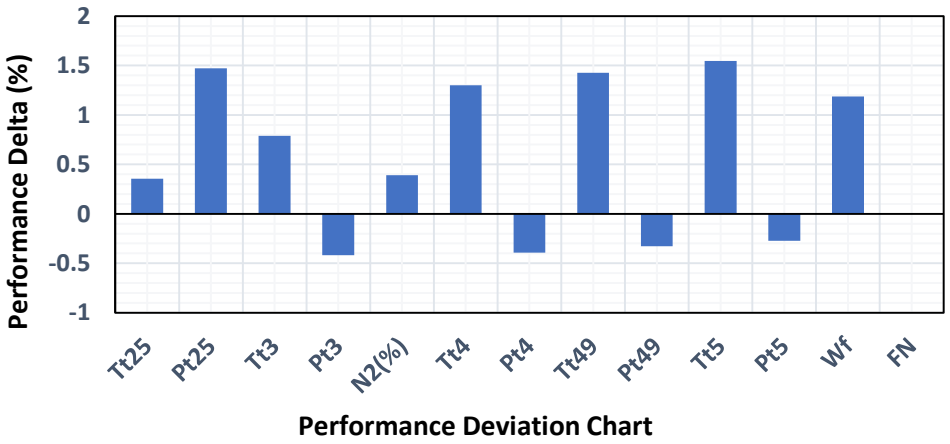

Figure (5.2): GPA of CF6-80C2 Engine GSP Model, Deteriorations Parameters Results for Case2

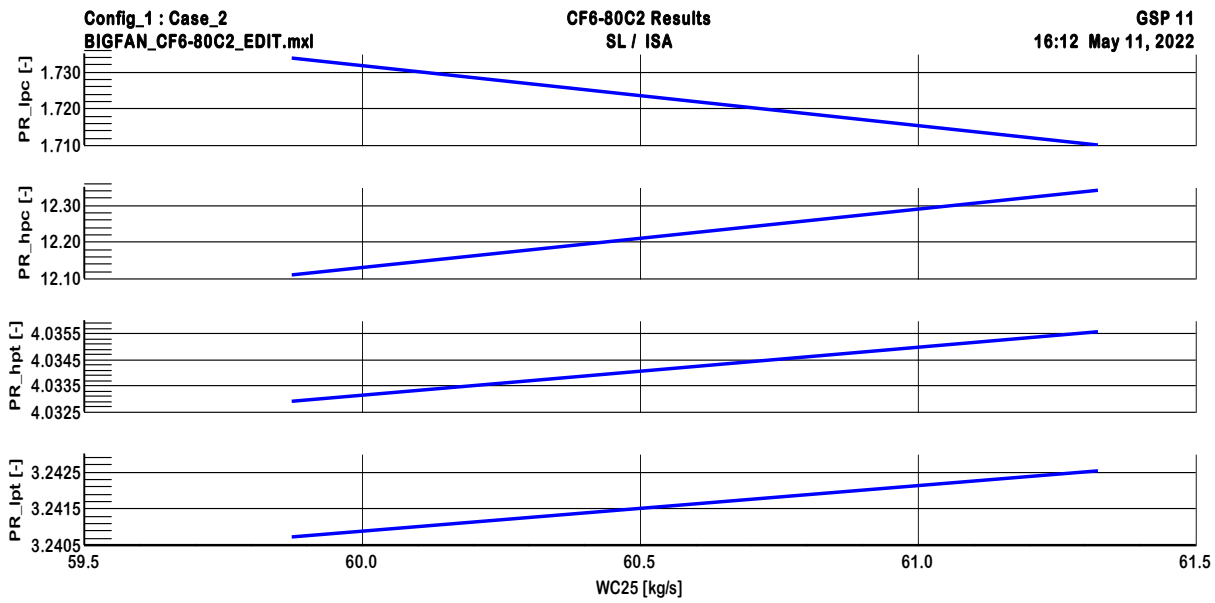

Figure (5.2a): GPA of CF6-80C2 Engine GSP Model, Changes of W25 with Engine Core Components Pressure Ratios for Case2

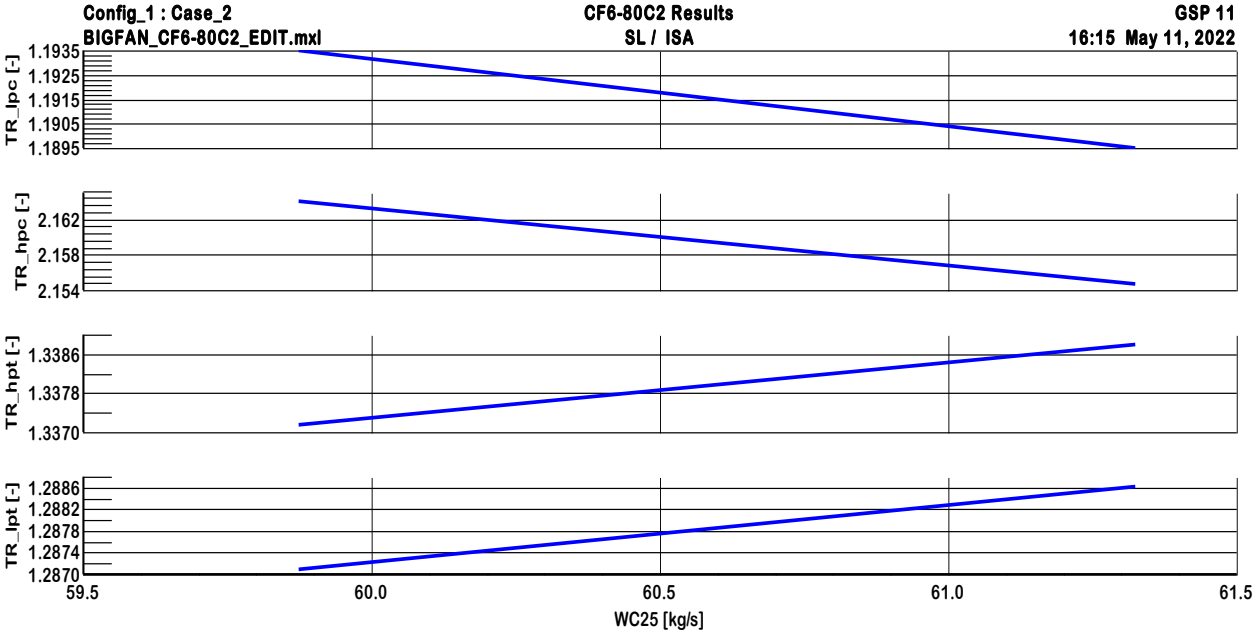

Figure (5.2b): GPA of CF6-80C2 Engine GSP Model, Changes of WC25 with Engine Core Components Temperature Ratios for Case2

Case3: HPT deteriorated in this case, by increasing the corrected mass flow rate (HPTWC), and decreasing isentropic efficiency (HPTη) as shown in table (5.1), representing the case of the eroded turbine. Due to decreasing in HPTη, spool speed (N2) was reduced by about 2.15%, and temperature ratio and difference over HPT decreased too, as EGT rose about 1.92% which leads to reduce the work delivered by HPT.

By investigating equation (2.4), and as it assumed that HPT is chocked, it is found that the ratio Tt_4/Tt_{25} increased, which caused an increase in fuel flow of about 1.55% as may note in figure (5.3). The LPC and LPT will keep turning at a constant speed, as is assumed the engine is N1 controlled, this will result in an increase in pressure ratio and temperature ratio over the LPC, while there aren't changes in pressure ratio and temperature ratio over LPT, as may note that in figure (5.3a) and (5.3b) respectively.

The thrust FN doesn't change, because of the increase in mass flow in HPT due to increasing the turbine nozzle guide vane area due to erosion, which will contribute to increasing the value of momentum thrust.

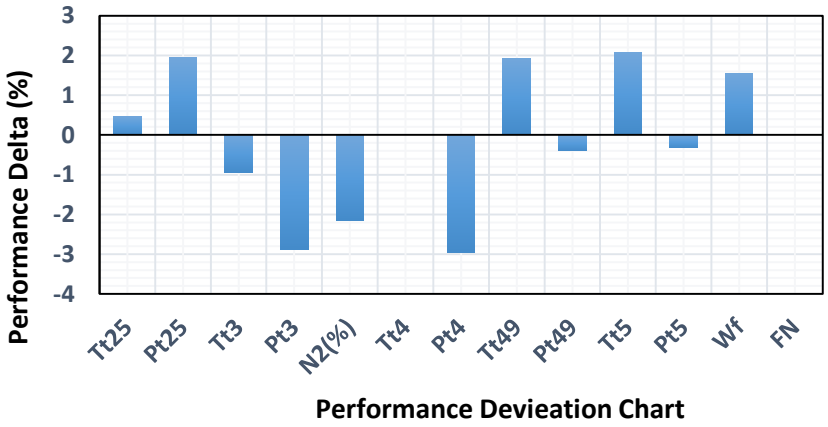

Figure (5.3): GPA of CF6-80C2 Engine GSP Model, Deteriorations Parameters Results for Case3

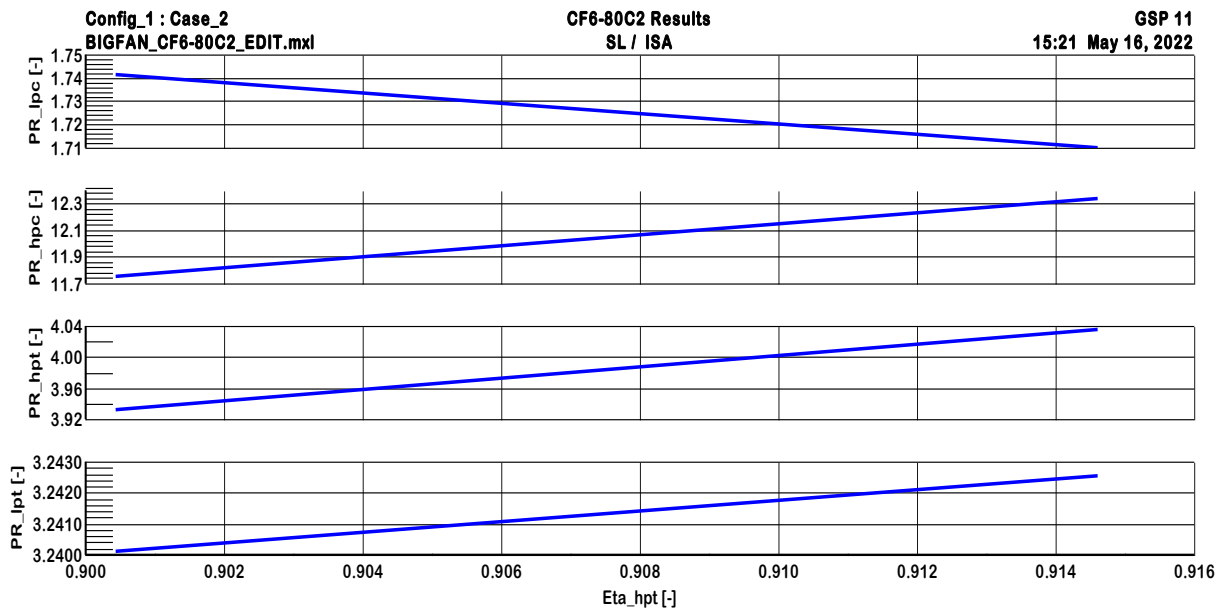

Figure (5.3a): GPA of CF6-80C2 Engine GSP Model, Changes of HPTη with Engine Core Components Pressure Ratios for Case3

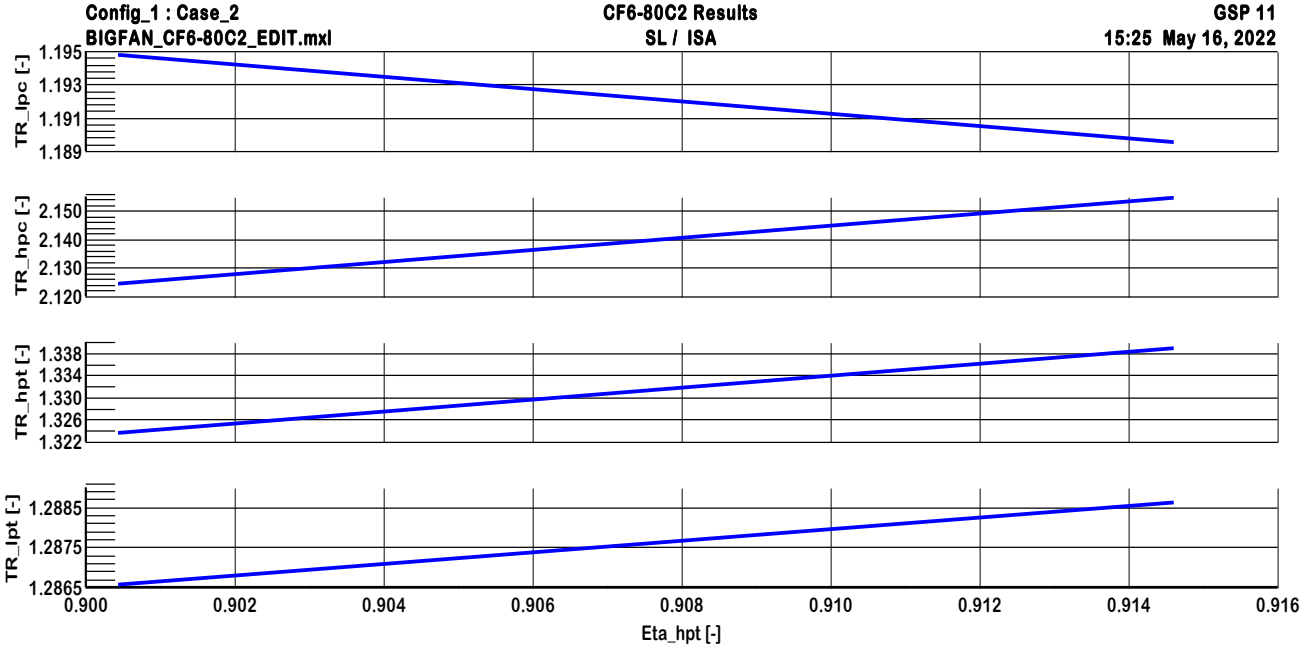

Figure (5.3b): GPA of CF6-80C2 Engine GSP Model, Changes of HPTη with Engine Core Components Temperature Ratios for Case3

Case4: LPT is deteriorated, by increasing the corrected mass flow rate ($LPTW_C$) and decreasing isentropic efficiency ($LPT\eta$), representing the eroded turbine. The assumed engine is N1 controlled, so the spool speed of the LPT will remain constant. As mentioned before that the engine is assumed N1 controlled, so the spool speed of the LPT will remain constant. To keep the N1 speed constant more energy will have to be added to the flow, increasing the fuel flow and EGT by about 3.6% and 1.6% respectively, as shown in figure (5.4). By considering equation (2.7), assuming that the HPT is chocked and operating at constant efficiency, it is found that with increasing LPT mass flow the HPT pressure ratio increased.

Increasing the dimensionless mass flow through the LPT leads to an increase in the effective area of the turbine nozzle guide vane, and due to the increase in HPTPR the HPT spool speed rose by about 1.82%. The increased spool speed N2 leads to an increase in the available mass flow through the HPC and increases the pressure ratio over the HPC, which will increase the work done in the HPC, allowing the work delivered by HPT to be increased too, as well as, the ratio Tt_4/Tt_{25} increased leads to increase fuel flow.

By investigating equations (2.5) and (2.7). The LPC is affected by the LPT as they are located on the same shaft N1, increases in LPT mass flow decrease the pressure ratio of LPC. The changes in the pressure ratios and temperature ratios are presented in figures (5.4a) and (5.4b) respectively.

The thrust FN increased by 0.87%, because of an increase in mass flow in LPT, due to increasing the turbine nozzle guide vane area, due to erosion, which will contribute to increasing the value of momentum thrust.

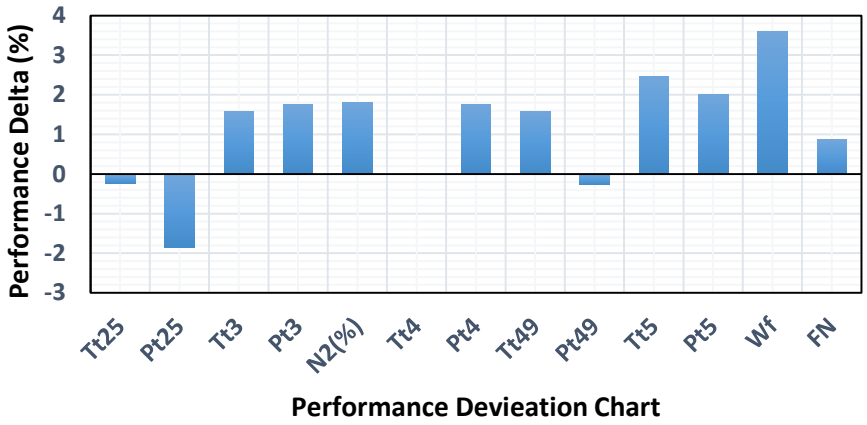

Figure (5.4): GPA of CF6-80C2 Engine GSP Model, Deteriorations Parameters Results for Case4

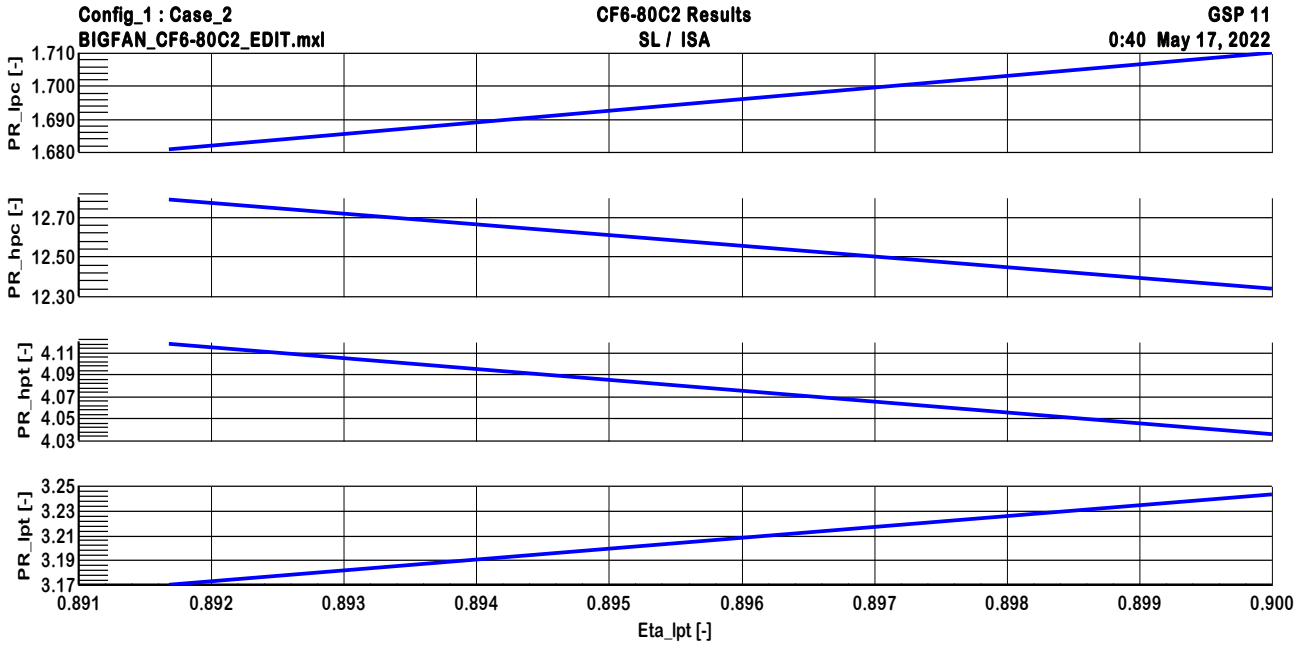

Figure (5.4a): GPA of CF6-80C2 Engine GSP Model, Changes of LPTη with Engine Core Components Pressure Ratios for Case4

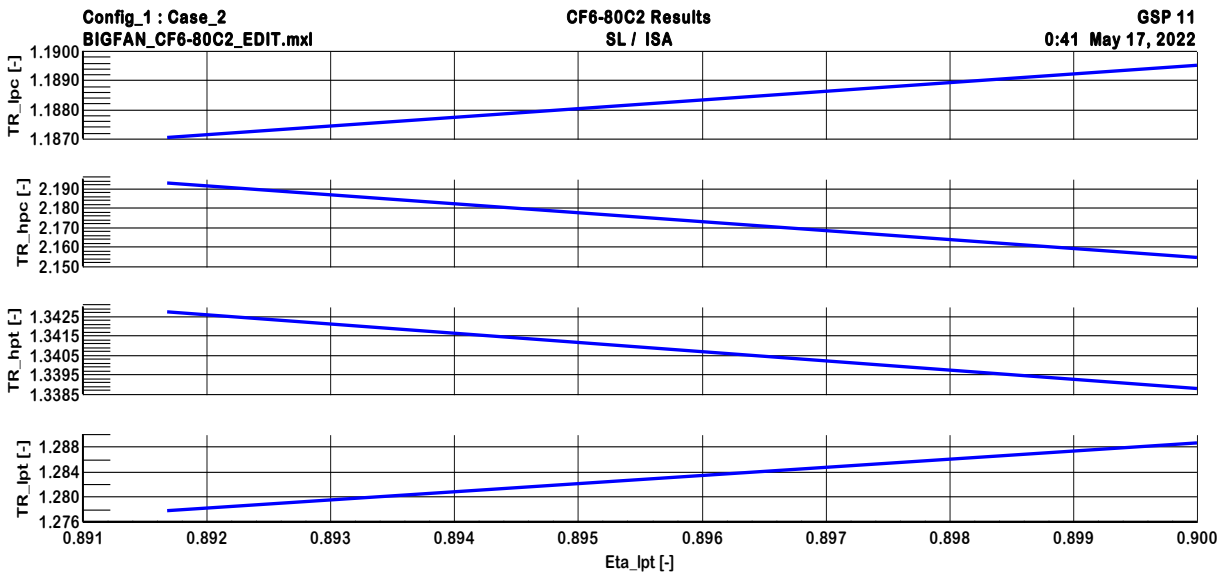

Figure (5.4b): GPA of CF6-80C2 Engine GSP Model, Changes of LPTη with Engine Core Components Temperature Ratios for Case4

5.2.2 RESULTS CATEGORY (II. CORE+)

Case5: Both LPC and HPC deteriorated, as presented in table (5.1), by decreasing the corrected mass flow WC and isentropic efficiency η in both compressors, due to physical problem as fouling in both compressors. So due to decreasing the mass flow in both LPC and HPC, the pressure ratios in both compressors are decreased as noted in figures (5.5a) and (5.5c). while the temperature ratios and differences in both compressors are increased due to decreasing isentropic efficiencies in both compressors, as noted in figures (5.5b), and (5.5d), which leads to an increase in the work done by both compressors, allowing the HPT and LPT to increase the work delivered by both of them, and also caused to increase the shaft speed N2 about 0.85%, and fuel flow about 1.37%, as EGT increased 2.28%, while the thrust decreased 0.25%, as shown in figure (5.5).

The changes in other parameters such as pressure ratios and temperature ratios due to deteriorations in LPC and HPC are as discussed before in case1 and case2, and shown in figures (5.5a), (5.5b), (5.5c), and (5.5d).

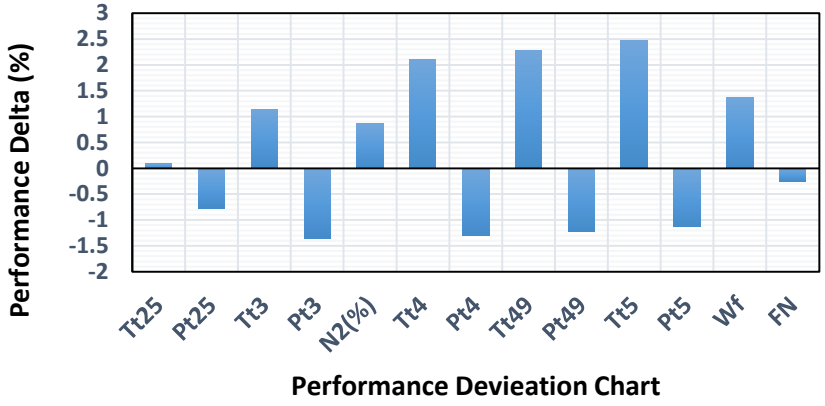

Figure (5.5): GPA of CF6-80C2 Engine GSP Model, Deteriorations Parameters Results for Case5

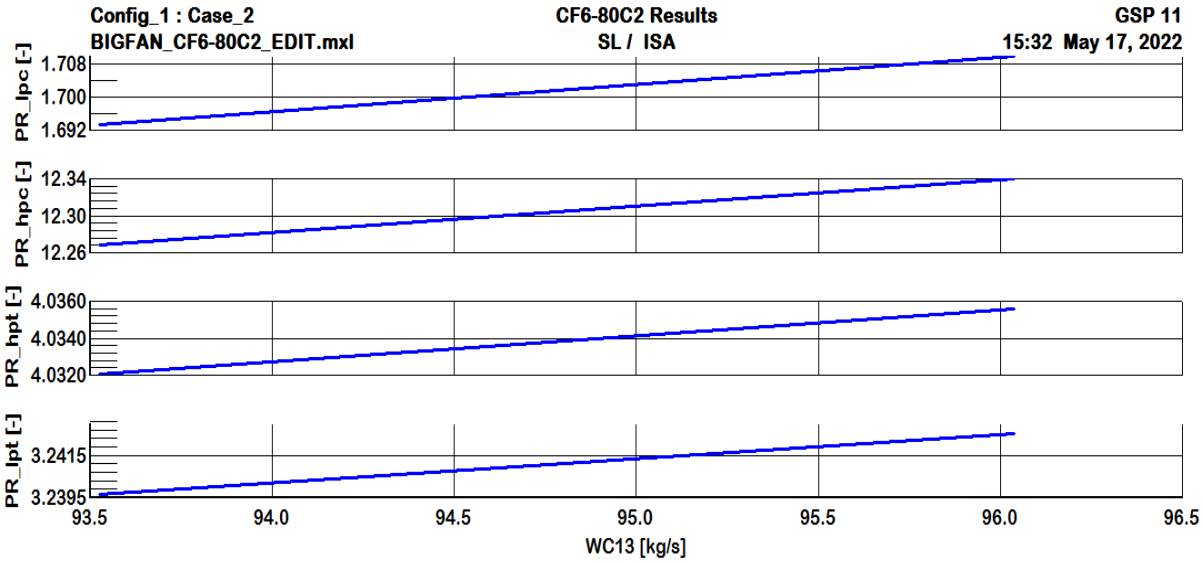

Figure (5.5a): GPA of CF6-80C2 Engine GSP Model, Changes of WC13 with Engine Core Components Pressure Ratios for Case5

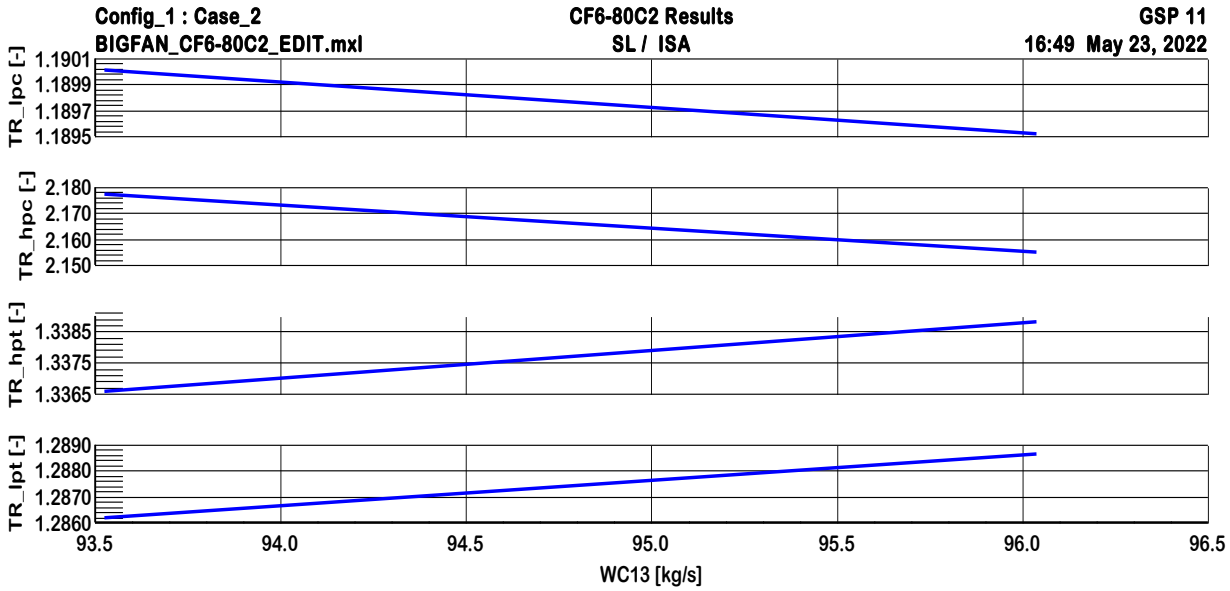

Figure (5.5b): GPA of CF6-80C2 Engine GSP Model, Changes of WC13 with Engine Core Components Temperature Ratios for Case5

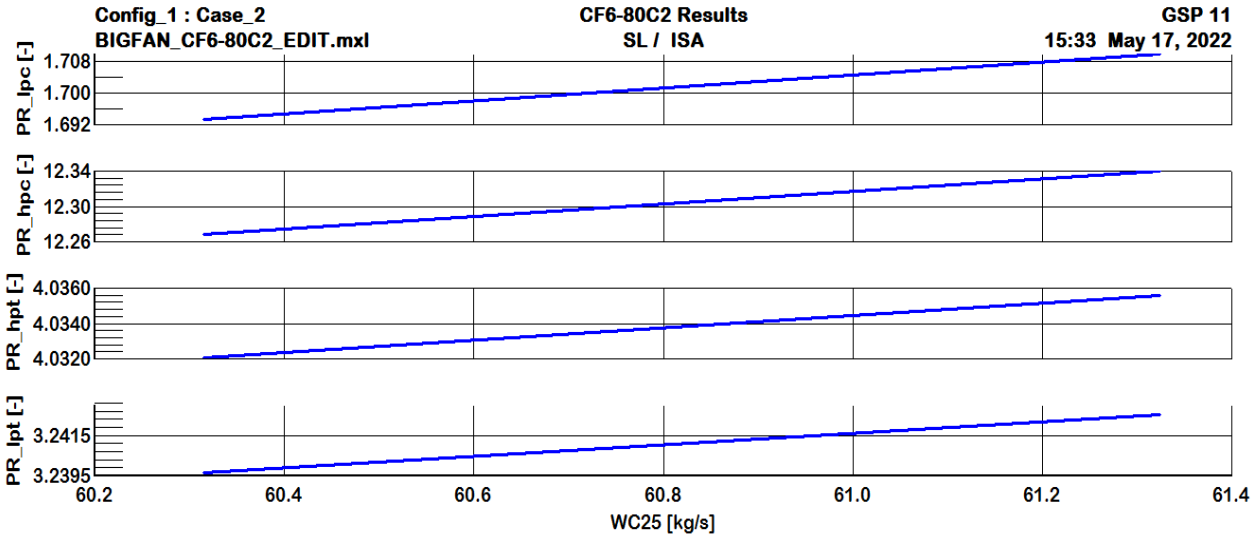

Figure (5.5c): GPA of CF6-80C2 Engine GSP Model, Changes of WC25 with Engine Core Components Pressure Ratios for Case5

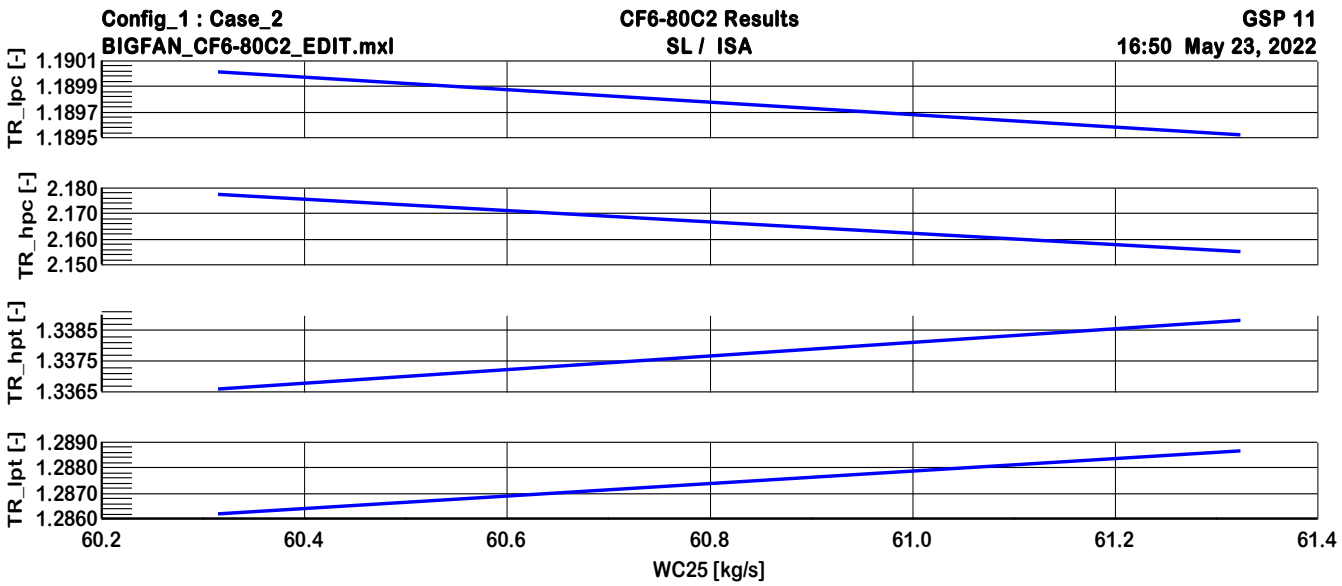

Figure (5.5d): GPA of CF6-80C2 Engine GSP Model, Changes of W25 with Engine Core Components Temperature Ratios for Case5

Case6: HPT and LPT deteriorated, by increasing the corrected mass flow rate in both turbines and decreasing the isentropic efficiency of both of them, representing the case of the eroded turbines. The fuel flow increased by about 4.18%, EGT increased by 2.26%, TIT (Tt4) increased by about 1.66%, and the thrust increases by about 0.95% due to an increase in the airflow in both turbines which contribute to an increase in the thrust. N2 is slightly increased. The changes in pressure ratios and temperature ratios due to deteriorations are presented in figures from (5.6a) to (5.6d).

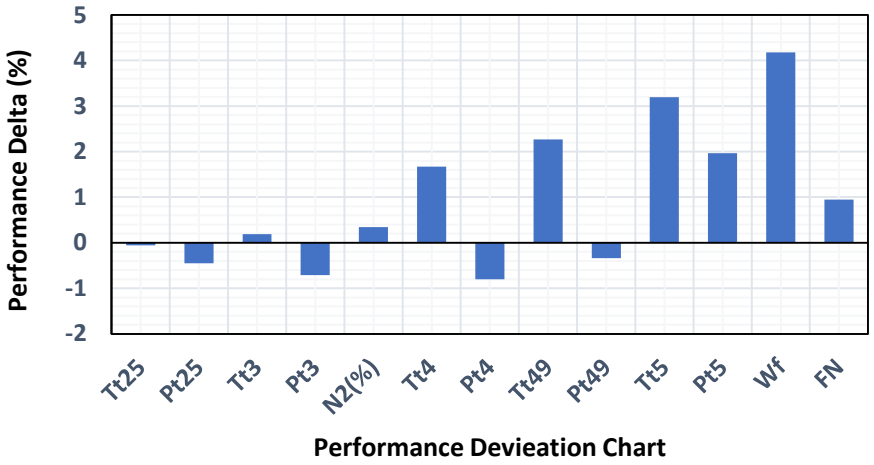

Figure (5.6): GPA of CF6-80C2 Engine GSP Model, Deteriorations Parameters Results for Case6

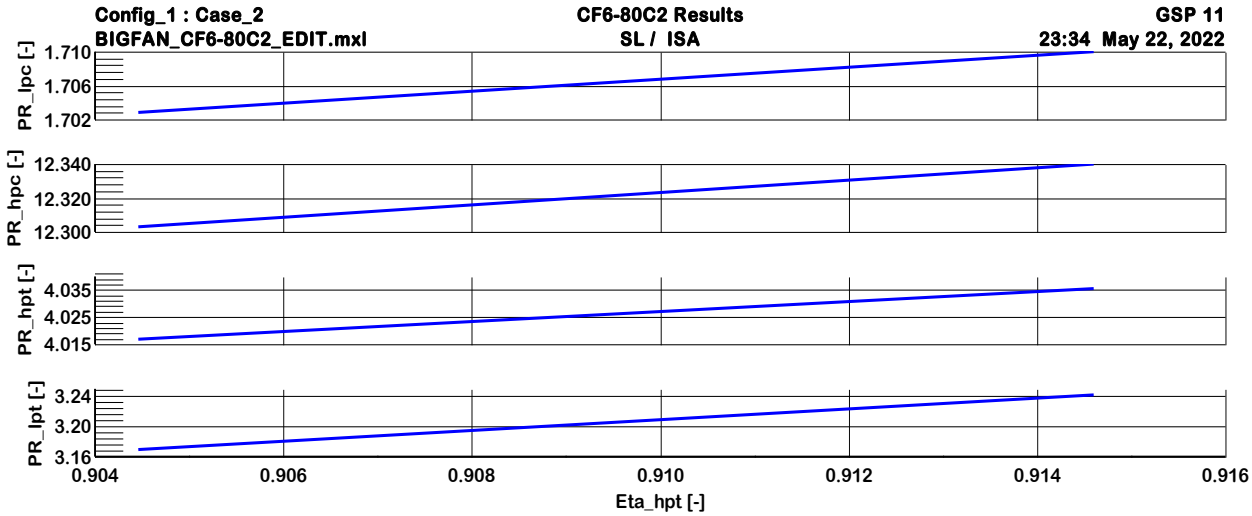

Figure (5.6a): GPA of CF6-80C2 Engine GSP Model, Changes of HPTη with Engine Core Components Pressure Ratios for Case6

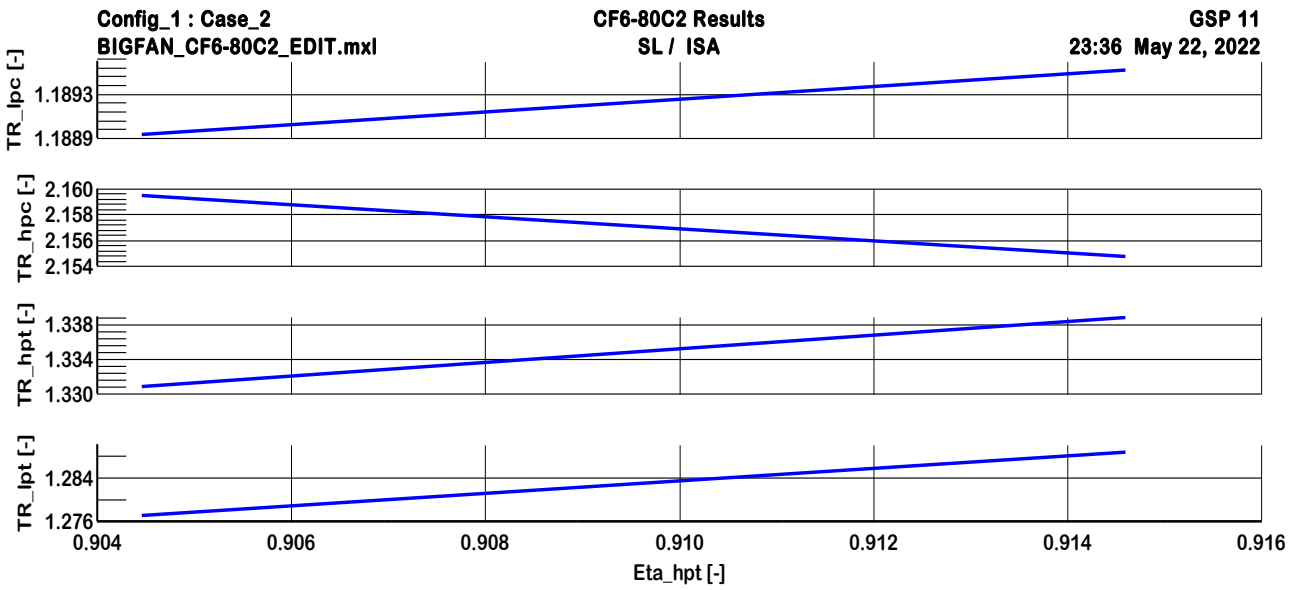

Figure (5.6b): GPA of CF6-80C2 Engine GSP Model, Changes of HPTη with Engine Core Components Temperature Ratios for Case6

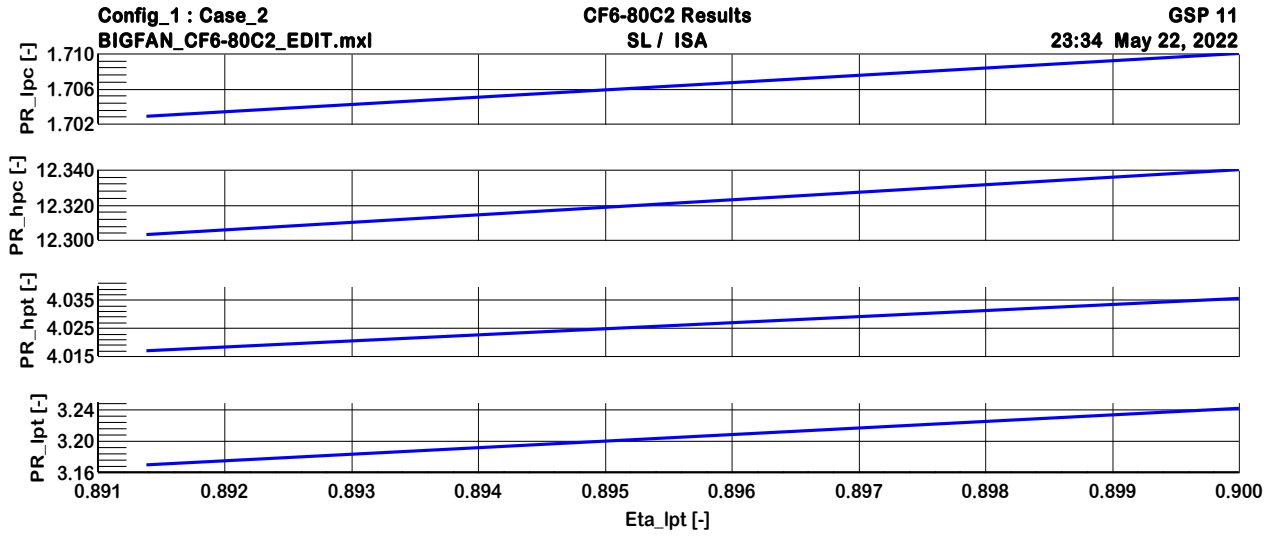

Figure (5.6c): GPA of CF6-80C2 Engine GSP Model, Changes of LPTη with Engine Core Components Pressure Ratios for Case6

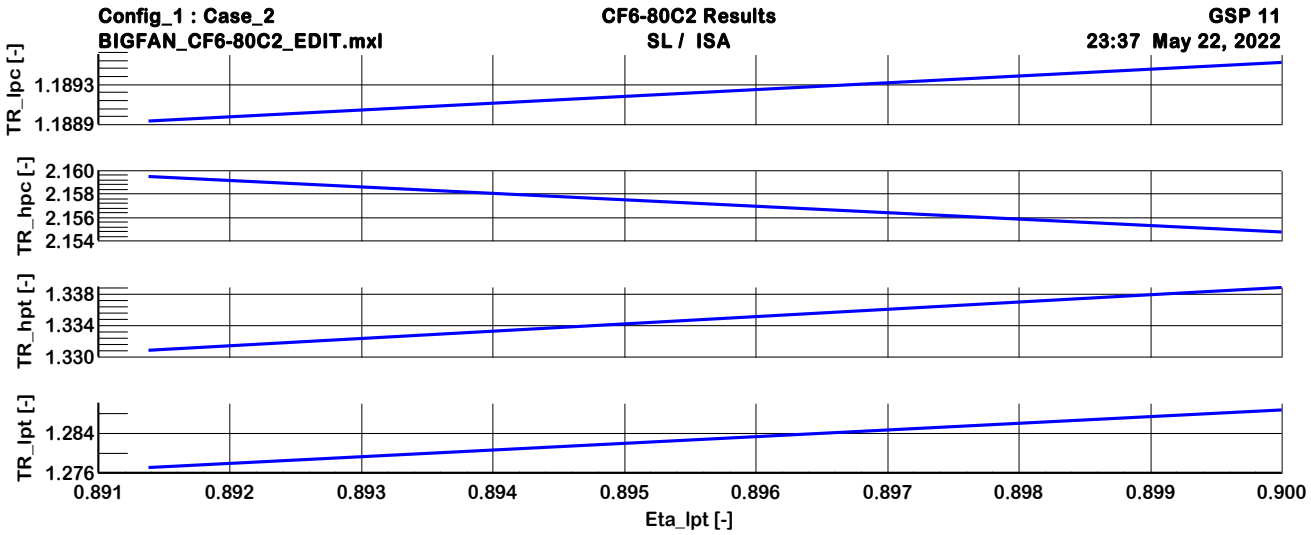

Figure (5.6d): GPA of CF6-80C2 Engine GSP Model, Changes of LPTη with Engine Core Components Temperature Ratios for Case6

Case7: LPC, HPC, HPT, and LPT deteriorated, by decreasing in corrected mass flow rate in LPC and HPC respectively, and increasing in corrected mass flow rate in HPT, and LPT respectively, and by decreasing in isentropic efficiency in all of them, representing the case of fouling in LPC, HPC, and eroded HPT, LPT. This case has the highest severity of engine deterioration, Wf, EGT, and N2 increased by about 5.58%, 4.62%, and 1.21% respectively, while FN increased by about 0.67% due to increasing the airflow in both turbines. Changes in pressure ratios and temperature ratios are presented in figures from (5.7a) to (5.7h).

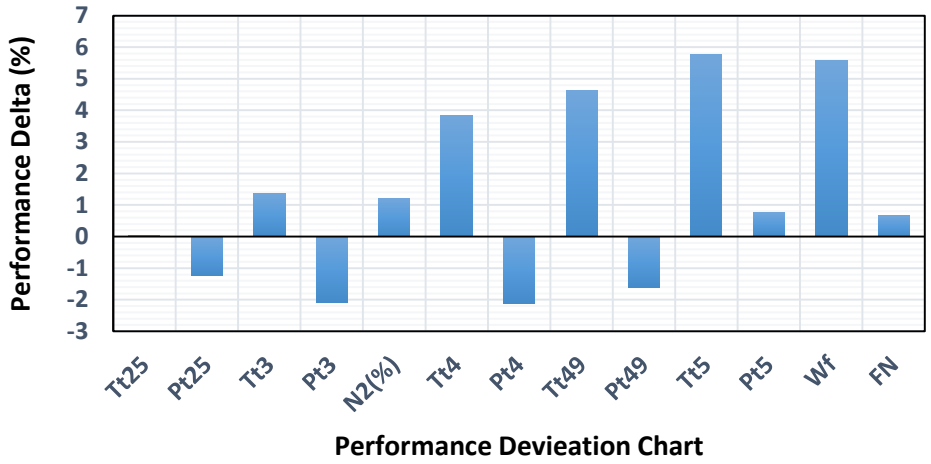

Figure (5.7): GPA of CF6-80C2 Engine GSP model, Deteriorations Parameters Results for Case7

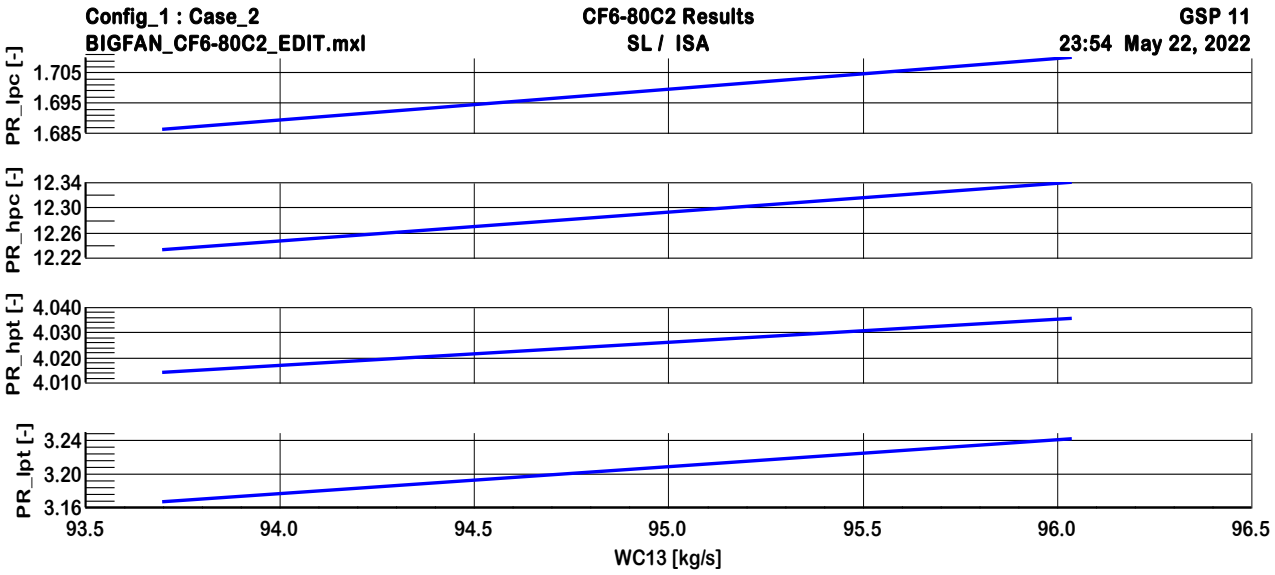

Figure (5.7a): GPA of CF6-80C2 Engine GSP Model, Changes of WC13 with engine core components pressure ratios for case7

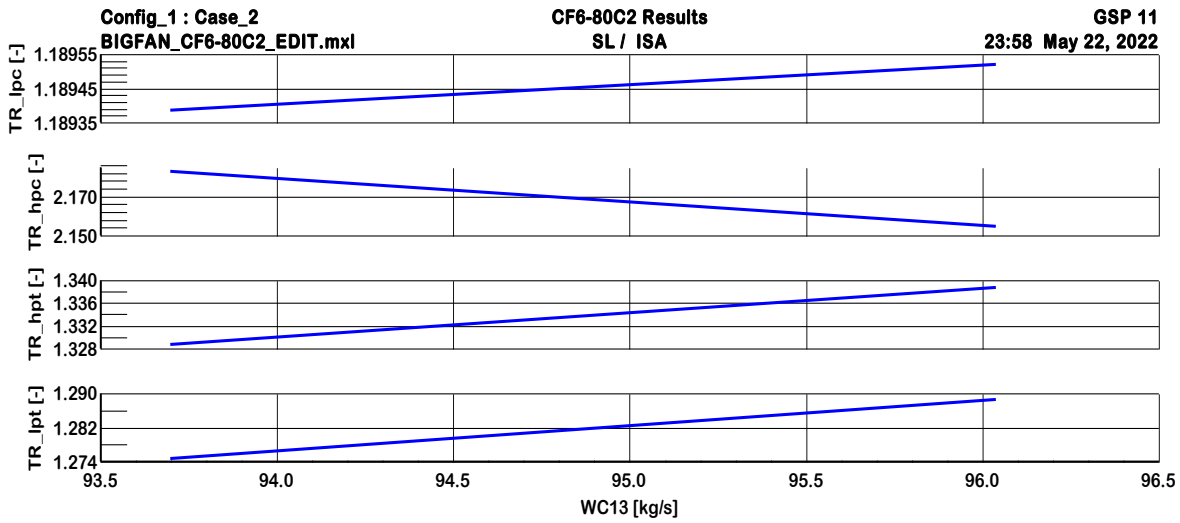

Figure (5.7b): GPA of CF6-80C2 Engine GSP Model, Changes of WC13 with Engine Core Components Temperature Ratios for Case7

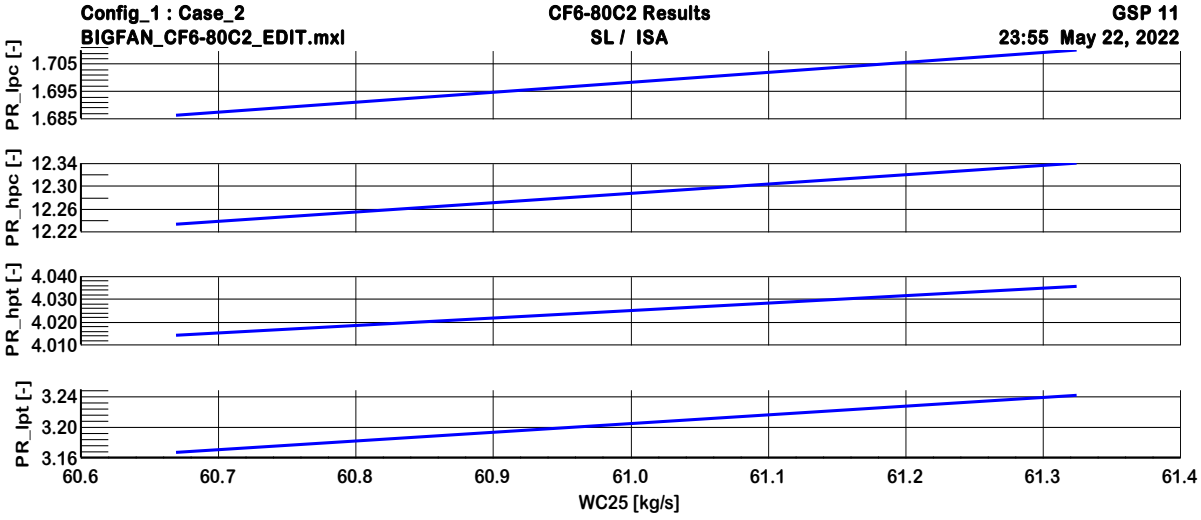

Figure (5.7c): GPA of CF6-80C2 Engine GSP Model, Changes of WC25 with Engine Core Components Pressure Ratios for Case7

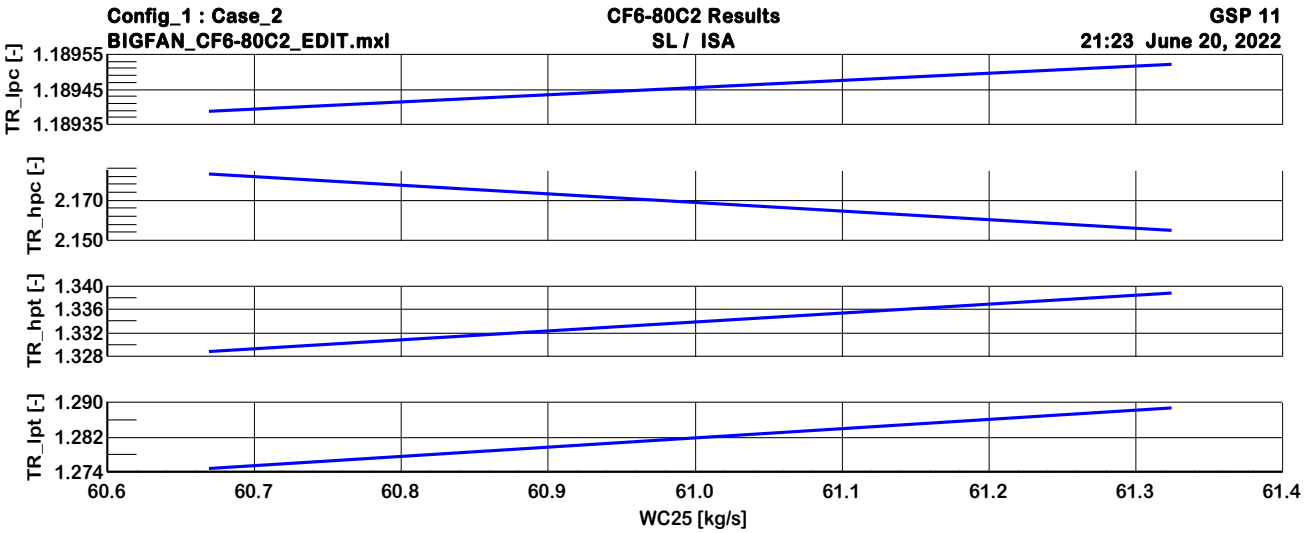

Figure (5.7d): GPA of CF6-80C2 Engine GSP Model, Changes of WC25 with Engine Core Components Temperature Ratios for Case7

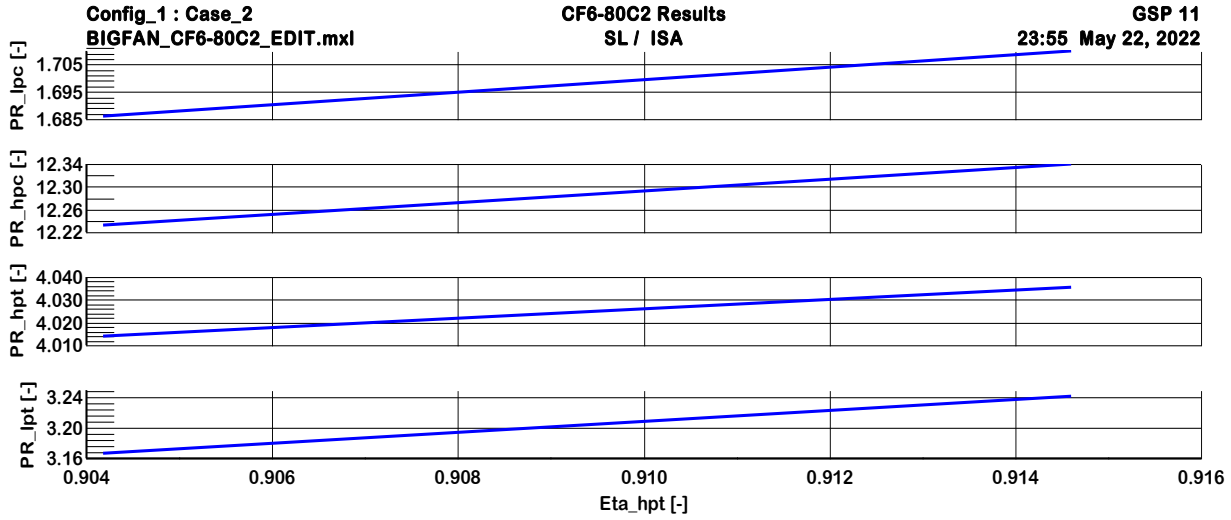

Figure (5.7e): GPA of CF6-80C2 Engine GSP Model, Changes of HPTη with Engine Core Components Pressure Ratios for Case7

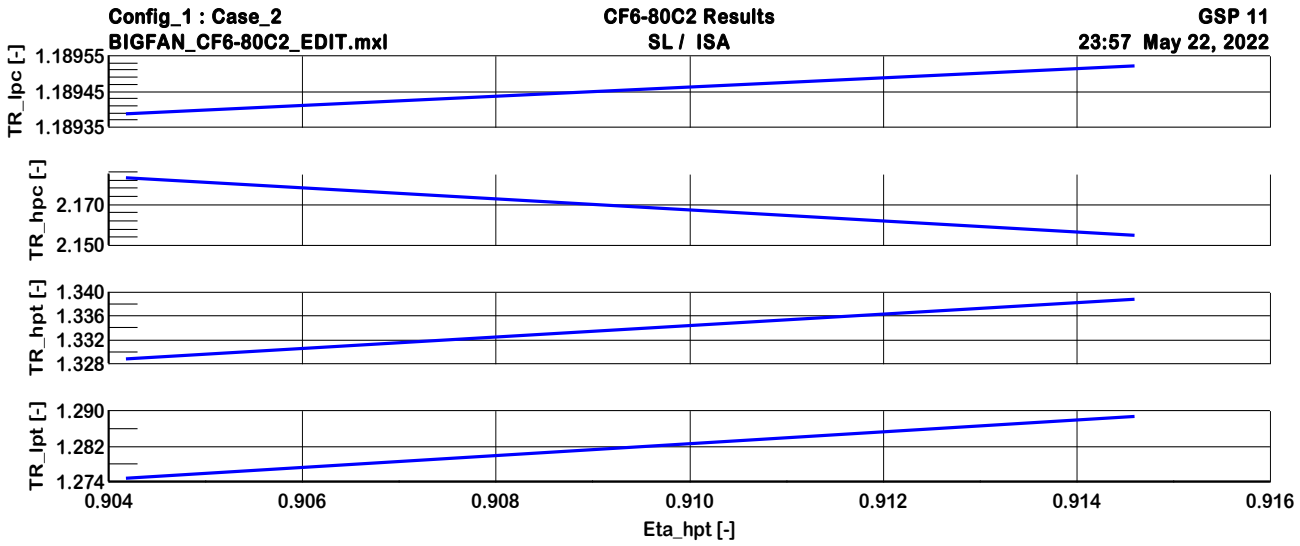

Figure (5.7f): GPA of CF6-80C2 Engine GSP Model, Changes of HPTη with Engine Core Components Temperature Ratios for Case7

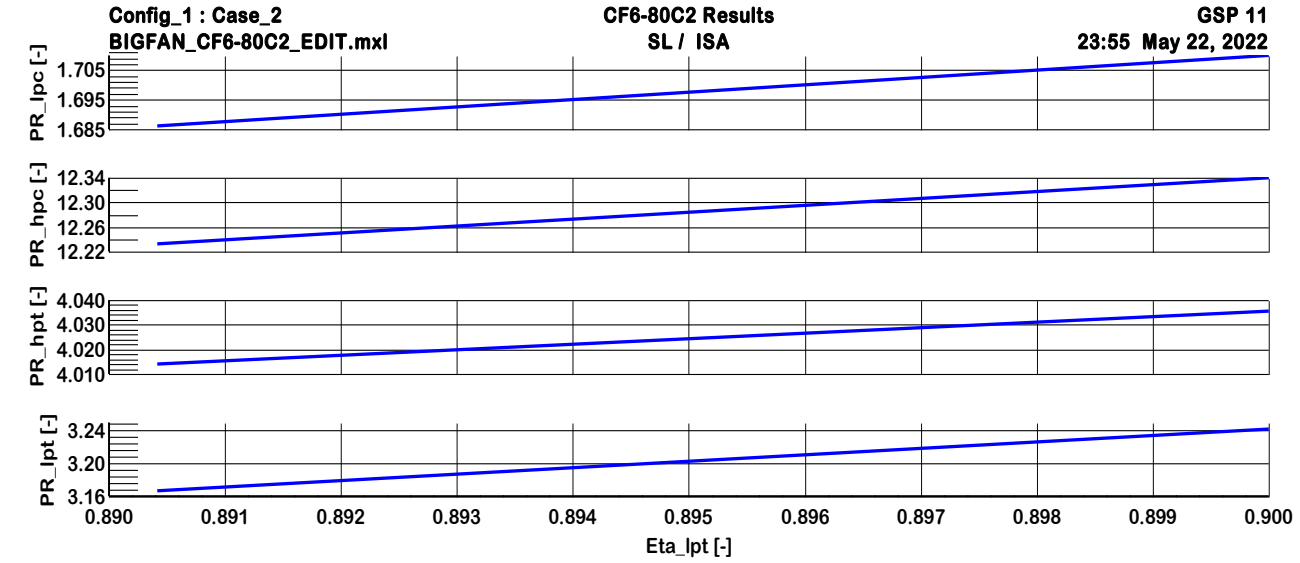

Figure (5.7g): GPA of CF6-80C2 Engine GSP Model, Changes of LPTη with Engine Core Components Pressure Ratios for Case7

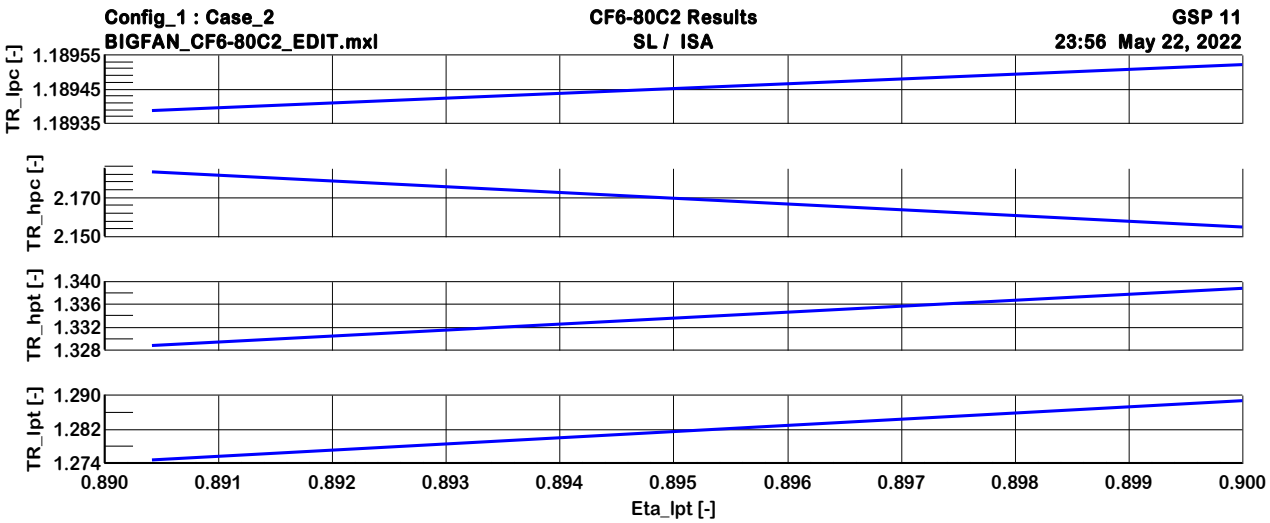

Figure (5.7h): GPA of CF6-80C2 Engine GSP Model, Changes of LPTη with Engine Core Components Temperature Ratios for Case7

5.2.3 EGT MARGIN OF THE CF6-80C2 ENGINE MODEL:

As mentioned in Chapter 1. The exhaust gas temperature (EGT) is the most important engine parameter used to monitor and analyze gas turbine performance. The difference between the measured EGT temperature and the EGT limit is called the exhaust gas temperature margin (EGT margin or EGTM). The aircraft operators are generally concerned with the EGT margin. CF6-80C2 Engine has maximum permissible EGT at Take-off which is 960C0 (1233 k) [21].

Figure (5.8) shows the EGT of the CF6-80C2 Engine Model deteriorated cases, studied with the presence of the Maximum EGT permissible of the Engine, which shows the EGT Margin at each case. The lowest engine EGT Margin shown was in case 7, which is 57.25 K. The engine in this case may be ordered for engine overhaul for the maintenance purposes.

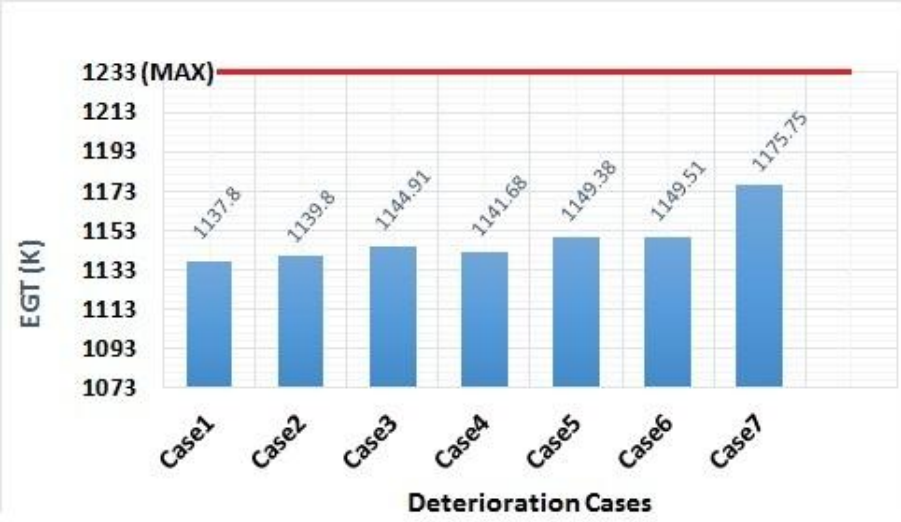

Figure (5.8): CF6-80C2 Engine Deteriorated Cases EGT Margin

5.2.4 RESULTS COMPARISON

A case study of the GPA experimental for the engine CF6-80C2 maintenance from [2], was selected as a comparison study with the GSP model. In this particular case study, the engine has some repairs in its core components, after that, the engine has run in a test cell at the take-off power setting. The bar chart in figure (5.9) shows the condition deltas of the repaired engine, these deltas are relative to the engine performance data shown in table (3.1). These condition deltas or deteriorated deltas are applied to the CF6-80C2 engine GSP model to compare the results of the model with the GPA experimental data.

Figure (5.10) shows the comparison between GSP model results with GPA experimental data to the same model of engine CF6-80C2 after applying the condition deltas of the engine, shown in figure (5.10). The results shown in figure (5.10) are a deviation from the reference data shown in table (3.1).

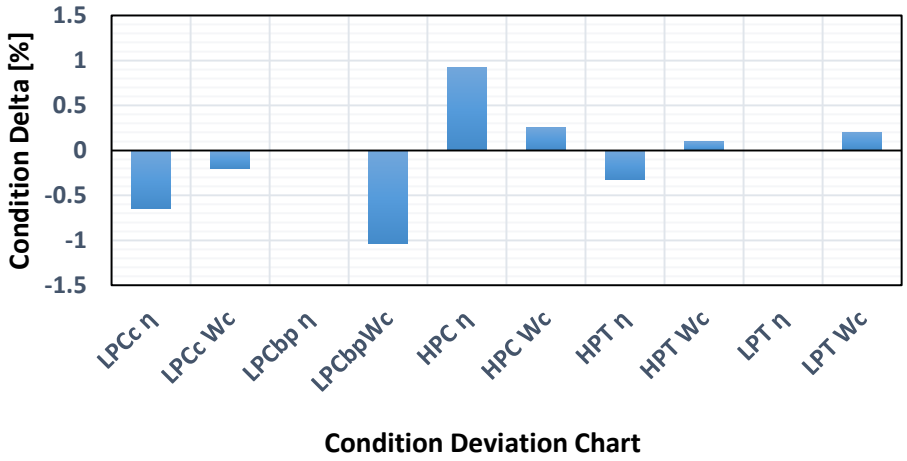

Figure (5.9): Condition Deltas of the CF6-80C2 Engine Model After Maintenance Repairs [2]

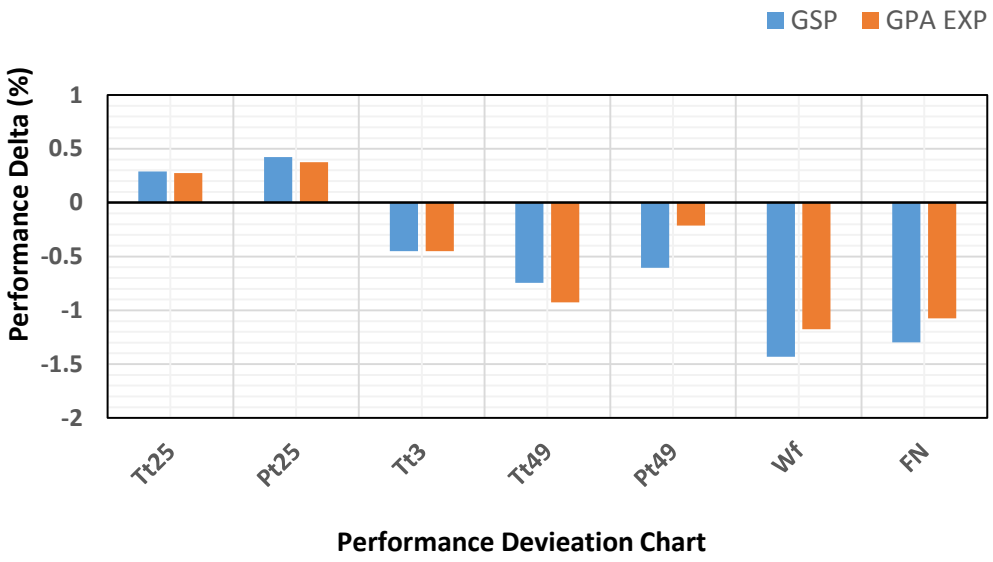

Figure (5.10): Comparison between GPA Exponential data and GSP Results of CF6-80C2 model

Table (5.2) shows the percentage difference between GPA Exponential data [2], and GSP results, the difference explanation between GSP results and GPA results is as the following equation (5.1).

$$Difference = \frac{GSP\ Result - GPA\ EXP\ Results}{\left(\frac{GPA\ EXP\ Results + GSP\ Result}{2}\right)} * 100 \quad \text{..... (5.1)}$$

Table (5.2): The Difference Between GPA EXP Data and GSP Results

Parameters (Unit)	**GPA EXP Data**	**GSP Model**	**Difference %**
Tt25 (K)	390.06975	390.1674349	0.025039788
Pt25 (Bar)	2.60272375	2.604198299	0.056638045
Tt3 (K)	834.229	834.5006608	0.032558998
Tt49 (K)	1112.61225	1115.40413	0.250615723
Pt49 (K)	7.5958245	7.566325596	-0.389112413
Wf (Kg/sec)	2.6583925	2.651463616	-0.260981985
FN (KN)	252.81273	252.2482143	-0.223543608

As it is shown in table (5.2), the difference between the GPA experimental data and the GSP model of the engine CF6-80C2, shows agreement in almost all parameters. The highest difference in Pt49 = -0.389%, which is a small number and doesn't affect the comparison of the results. The other parameters have an agreement between the GPA experimental data and GSP results of the engine model.

The comparison between the GSP model and GPA experimental data of the CF6-80C2 model at off-design deteriorated in a take-off power setting as it is shown in table (7.2). The GSP model represents that the model is well, staying with +/- 0.39% as the maximum difference range for all measured parameters that are compared. As overall results, the GSP model is good enough to be usable, as expected that the GSP model results from comparison showed good agreement with GPA experimental data.

CHAPTER 6

CONCLUSIONS AND RECOMMENDATIONS

This chapter forms the end of the thesis, summarizing the conclusions made. Furthermore, a look is taken towards future researches with a number of recommendations.

6.1 CONCLUSIONS

Throughout the thesis, several conclusions have been drawn, either on the modeling of the design point or off-design deterioration of the model CF6-80C2. Below these conclusions will be reported.

1. Fewer gas path measurements are available on the CF6-80C2 engine, such as lacking a pressure measurement fan core (between fan core and booster(Pt13)), after the HPC (Pt3), and in the fan bypass duct (Pt14), and after LPT (Pt5). Furthermore, TT4 and Tt5 measurement is not available. This has influenced the design point modeling of the CF6-80C2 engine.
2. A design point model has been created, modeling the engine according to the test cell at the take-off power setting. Assumptions have been made on some component performance to compensate for the missing measurements. The computed component design conditions match closely to the GPA reference data.

3. The off-design model has been modeled for cruising speed 0.8 Mach number and at 10000m altitude to test the usability of the model and show the component characteristics scaled maps, as the CF6-80C2 component maps are unavailable outside the OEM environment.
4. Despite the unavailability of the original component maps, the off-design performance of the CF6-80C2 can be simulated well using the publicly available maps. The CF6-80C2 (Fan core and bypass) is isolated and each has its own map due to the difficulty to combine them on one map as the reference [2] did.
5. Results for the LPT represents the reduction in performance with contributed to the HPT, depending on the change in LPT mass flow capacity especially when the mass flow rate is increased in the LPT as may note in case 4.
6. Results for HPC deterioration shows more severity than in LPC as may note that in case 1 and case 2, the compressors are most affected by fouling, especially the HPC due to the higher temperatures.
7. The results for combined deteriorations from case5 to case 7, show more deteriorations severity than when single component degradation, which is clearer to note in the figures of the cases from case 5 to case 7.
8. In this thesis, it could be concluded that the GPA using the GSP program has shown good results for the CF6-80C2 model and other aero engines models, the results are good enough to study the deteriorations happened in the engine CF6-80C2 due to physical problems that mentioned in chapter 2.

6.2 RECOMMENDATIONS

Although this thesis has led to a working GSP model of CF6-80C2, which is used to analyze the deterioration of the model, more work is still to be done. Furthermore, the model can be used for further analysis in the future. Below some recommendations are given for improvements and future applications.

1. The components maps used in the CF6-80C2 model, were generic components maps scaled in the GSP to the engine-selected design point. Generating components maps for the engine are important to get a more accurate representation of CF6-80C2 performance.
2. It is recommended to measure the engine performance at more than one power setting, such as maximum continuous power setting, and cruise power setting, in the engine test cell when it is available in my country Libya, and compare the results with engine on-wing, where the information on how the engine behaves at different power settings. This would also allow for accurate performance engine study and to diagnose the engine health for maintenance purposes for aero-engines as general.
3. As mentioned in chapter 2, adaptive modeling AM has the facilities and capabilities of modeling virtually any gas turbine configuration. It is recommended to study and program this method to adapt the engine model to more accurate measured performance, which can be used to diagnose the engine models for gas path analysis which is important for maintenance purposes.

REFERENCES

[1]. M. P. R. van Moorselaar. Gas Path Analysis on the GEnx-1B at KLM Engine Services, Master thesis, Delft University of Technology, 2018.

[2]. ML Verbist. Gas Path Analysis for Enhanced Aero-Engine Condition Monitoring and Maintenance. PhD thesis, Delft University of Technology, 2017.

[3]. GSP Development Team. GSP 11 User Manual. National Aerospace Laboratory NLR, October 2013.

[4]. GSP team. Gas turbine simulation program. https://www.gspteam.com/.

[5]. HIH Saravanamuttoo, GFC Rogers, H Cohen, and PV Straznicky. Gas Turbine Theory. Pearson Education, 7th edition, 2017.

[6]. Philip P. Walsh, Paul Fletcher. Gas Turbine Performance. Second Edition, 2004.

[7]. H. Pieters Gas Path Analysis with GSP for the GEM42 turboshaft engine, Delft University of Technology, 2005.

[8]. GE Aircraft Engines. CF6-80C2 high-bypass turbofan engines.

[9]. Several authors and contributors. Performance prediction and simulation of gas turbine engine operation. Technical report, Research and Technology Organisation NATO, 2002. RTO-TR-044.

[10]. Anish Mathew Sajeev. Gas Turbine Diagnostics Based on Gas Path Analysis, Master Thesis, Delft University of Technology, 2015

[11]. Instituto Tecnológico de Aeronáutica (ITA), São José dos Campos, Brazil. Part42: Applied Topics On Aircraft Propulsion, 5- Engine Deterioration & Health Monitoring, 2016.

[12]. Ivan Hutter, GE imagination at work. Engine Deterioration and Maintenance Actions, 2006. Conference Paper in ICAO / Transport Canada Conference, Aircraft Panel, Montreal, September 2006.

[13]. Rainer Kurz, Klaus Brun. Fouling Mechanism in Axial Compressors. Conference Paper in Journal of Engineering for Gas Turbines and Power · January 2011.

[14]. Jasem Alqallaf, Naser Ali, Joao A. Teixeira, and Abdulmajid Addali. Solid Particle Erosion Behavior and Protective Coatings for Gas Turbine Compressor Blades. Research Paper August 2020.

[15]. P. C. Escher. Pythia: An Object-Oriented Gas Path Analysis Computer Program for General Applications, PhD thesis, Cranfield University, School of Mechanical Engineering, 1995.

[16]. A Stamatis, K Mathioudakis, and KD Papailiou. Adaptive simulation of gas turbine performance. ASME Journal of Engineering for Gas Turbines and Power, 112(2):168–175, 1990.

[17]. GKN Aerospace, GE CF6-80C2 STAGE 1 FAN BLADE.

[18]. Paolo Lironi. CF6-80C2 engine history and evaluation, International Aviation Services Group, Engine Yearbook 2007.

[19]. GE Aircraft Engines. CF6-80C2 Engine Review, Flight Operations FADEC Version.

[20]. Philip Hill, Carl Peterson. Mechanics and Thermodynamics of Propulsion. Second Edition, 1992.

[21]. European Union Aviation Safety Agency (EASA). Type-Certificate Data Sheet for CF6-80A / CF6-80C Series, 11 April 2022.

[22]. Muhammad Naeem. Implications of Aero-Engine Deterioration for a Military Aircraft's Performance. PhD thesis, Cranfield University, School of Mechanical Engineering, April 1999.

APPENDIX A

CF6-80C2 VARIANTS

CF6-80C2 is the most successful generation of the CF6 engines and has acquired the highest market share on all the aircraft types it powers [18]. Table (A.1) shows the variants of the CF6-80C2 engine.

Table (A.1): CF6-80C2 Engine Variants

Engine Model	Thrust Rating (KN)	Flat Rated Temperature (C^0)	Aircraft Type
CF6-80C2A1	262.45	30	A300B4-600
CF6-80C2A2	237.98	43.89	A310-200/-300
CF6-80C2A3	267.78	30	A300B4-600
CF6-80C2A5	272.68	30	A300B4-600R
CF6-80C2A5F	272.68	30	A300B4-600R
CF6-80C2A8	262.45	35	A310-300
CF6-80C2B1	252.21	30	VC25,B747-300
CF6-80C2B1F	258.4	32.22	B747-400
CF6-80C2B2	233.53	32.22	B767-200/-300
CF6-80C2B2F	234.42	32.22	B767-200/-300

CF6-80C2B4	257.55	32.22	B767-200/-300
CF6-80C2B4F	257.55	32.22	B767-200/-300
CF6-80C2B5F	270.45	30	B767-200/-300
CF6-80C2B6	270.45	30	B767-300
CF6-80C2B6F	270.45	30	B767-200/-300
CF6-80C2B7F	270.45	30	B767-200/-300
CF6-80C2B8F	275.61	30	B767-400
CF6-80C2D1F	275.61	30	MD11

APPENDIX B

ADDITIONAL SIMULATED DETERIORATIONS RESULTS

Tens of engine deterioration cases can be applied in the studied model. In this appendix, the cases of engine fan degradation with degradation of both HPT and LPT will be presented, by decreasing the mass flow in both of them. Table (b.1) shows simulated deteriorations cases added to the CF6-80C2 model.

Table (B.1): Additional Simulated Deterioration Cases on CF6-80C2

Case	Fan Core		Fan Duct		LPC		HPC		HPT		LPT	
	$\Delta\eta$	ΔW_C	$\Delta\eta$	ΔW_C	$\Delta\eta$	ΔW_C	$\Delta\eta$	ΔW_C	$\Delta\eta$	ΔW_C	$\Delta\eta$	ΔWC
8	-0.33	-1	-1	-3								
9	-0.33	-1	-1	-3	-1	-3	-1	-3	-1	-2	-1	-2
10	-0.33	-1	-1	-3	-1	-3	-1	-3	-1	2	-1	2

Case 8: Figure (b.1) shows the results of deteriorated Fan (Core + Duct or Bypass), which represent fouled Fan. As presented in figure (b.1), all engine parameters almost decreased.

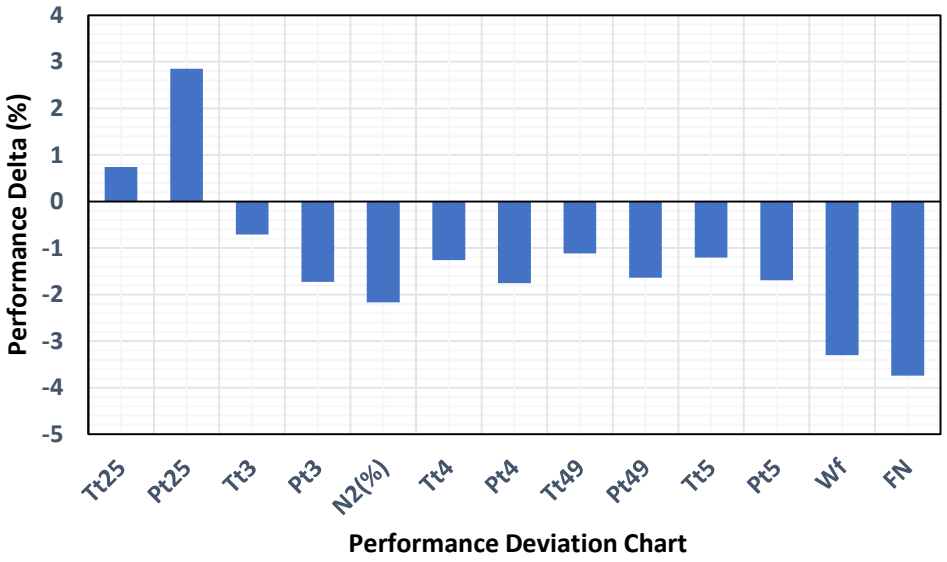

Figure (B.1): GPA of CF6-80C2 Engine GSP Model, Deteriorations Parameters Results for Case8

Case9: Figure (b.2) shows the results of the deteriorated fan, added to the combined deteriorated case with decreasing mass flow rate in both HPT and LPT.

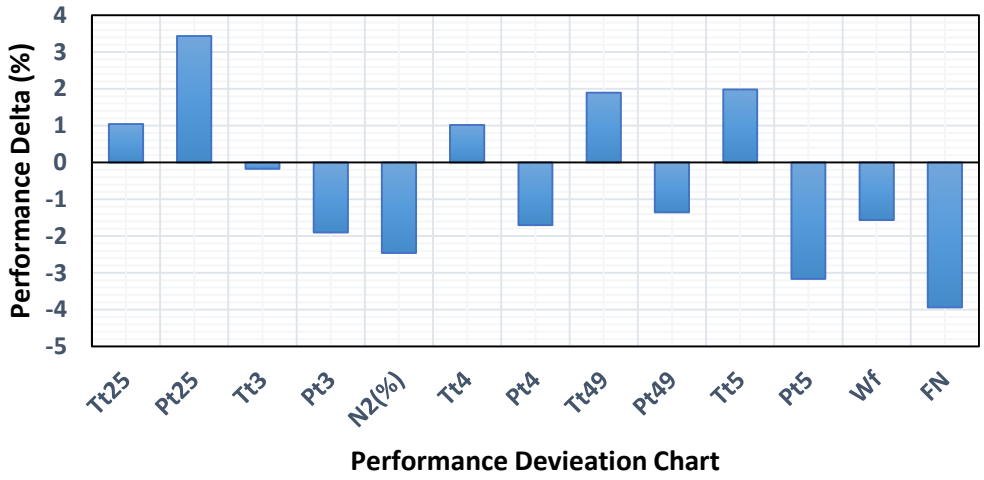

Figure (B.2): GPA of CF6-80C2 Engine GSP Model, Deteriorations Parameters Results for Case9

Case 10: Figure (b.3) shows the results of the deteriorated fan, added to the combined deteriorated case with increasing mass flow rate in both HPT and LPT.

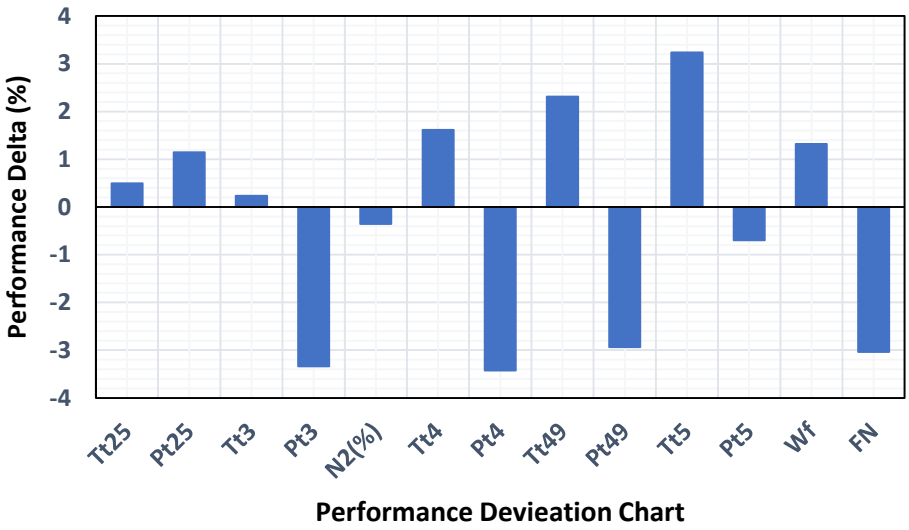

Figure (B.3): GPA of CF6-80C2 Engine GSP Model, Deteriorations Parameters Results for Case10

APPENDIX C

DESIGN POINT PERFORMANCE FOR TWIN-SPOOL UNMIXED TURBOFAN ENGINE

Design point calculations are relatively straightforward and can usually be completed without the need for iteration [1]. Design point calculations follow the air through the engine from the inlet to the nozzle. In this section, the design point calculations are shown. The exact equations to be used depending on the parameters known. Different authors use different schemes, however, the idea behind the equations is the same [1]. Station numbers are denoted as shown in figure (2.6).

First, the total ambient conditions have to be calculated, the total pressure P_{0a} and T_{0a} total temperature. This is done using equations (C.1) and (C.2).

$$T_{0a} = T_a \left(1 + \frac{\gamma_a - 1}{2} M^2\right) \quad \text{(C.1)}$$

$$P_{0a} = P_a \left(\left(1 + \frac{\gamma_a - 1}{2} M^2\right)^{\frac{\gamma_a}{\gamma_a - 1}}\right) \quad \text{(C.2)}$$

The ambient properties do not change at the start of the intake. The intake is assumed to be adiabatic, hence the total temperature remains constant over the intake. The total pressure changes. The total pressure after the intake is calculated using equation (C.3). Here η_{in} is the intake isentropic efficiency [1].

$$P_{02} = P_a \left(\left(1 + \eta_{in} \frac{\gamma_a - 1}{2} M^2 \right)^{\frac{\gamma_a}{\gamma_a - 1}} \right) \quad \text{(C.3)}$$

Next, the fan will compress the flow, increasing the total pressure and temperature. The pressure increase is dictated by the Pressure Ratio (PR) shown in equation (C.4). The temperature increase is dictated by the isentropic compression equation, with the added isentropic efficiency, equation (C.5). to simplify the calculations, assume that $P_{013} = P_{014}$ and $T_{013} = T_{014}$.

$$P_{013} = PR_{fan} . P_{02} \quad \text{(C.4)}$$

$$T_{013} = T_{02} \left(1 + \frac{1}{\eta_{fan}} \left(\left(\frac{P_{013}}{P_{02}} \right)^{\frac{\gamma_a - 1}{\gamma_a}} - 1 \right) \right) \quad \text{(C.5)}$$

After the fan, the airflow is split into the core and bypass flow. The bypass flow properties will not change anymore, and no pressure losses in the duct are taken into account in these calculations. The mass flow in both the core and bypass flow can be calculated using equation (C.6). Here it is assumed that the bypass ratio (BPR) is known and either the total mass flow, core mass flow, or bypass mass flow [1].

$$BPR = \frac{\dot{m}_{bypass}}{\dot{m}_{core}} \quad \text{(C.6)}$$

The core flow continues through the booster and HPC. Through both components the total pressure and temperature rise. The same equations as for the fan can be used, equations (C.7), (C.8), (C.9), and (C.10) replacing the fan PR and efficiency with those of the booster and HPC.

$$P_{025} = PR_{booster} . P_{013} \quad \text{(C.7)}$$

$$T_{025} = T_{013}\left(1 + \frac{1}{\eta_{booster}}\left(\left(\frac{P_{025}}{P_{013}}\right)^{\frac{\gamma_a - 1}{\gamma_a}} - 1\right)\right) \quad \text{(C.8)}$$

$$P_{03} = PR_{HPC}.P_{025} \quad \text{(C.9)}$$

$$T_{03} = T_{025}\left(1 + \frac{1}{\eta_{HPC}}\left(\left(\frac{P_{03}}{P_{025}}\right)^{\frac{\gamma_a - 1}{\gamma_a}} - 1\right)\right) \quad \text{(C.10)}$$

After the HPC, the core flow goes through the combustion chamber. In the combustion chamber pressure losses ΔP_{cc} occur due to friction and heat addition. These losses are assumed to be known, hence the total pressure after the combustion chamber is given by equation (C.11). Assuming that the fuel mass flow $\dot{m}_f$ is given, the total temperature inlet to HPT can be calculated with equation (C.12). Here η_{cc} is the combustion efficiency, C_{pg} specific heat of the gas, C_{Pa} specific heat of the air, and LHV_f is the lower heating value of the fuel. The total mass flow after the combustion chamber is given by equation (C.13).

$$P_{04} = P_{03} - \Delta P_{cc} \quad \text{(C.11)}$$

$$T_{04} = T_{03} + \frac{\dot{m}_f \; LHV_f \, \eta_{cc}}{\dot{m}_{core} \, C_{pg}} \quad \text{(C.12)}$$

$$\dot{m}_g = \dot{m}_4 = \dot{m}_{core} + \dot{m}_f \quad \text{(C.13)}$$

The HPT must provide the work needed by the HPC. Using equation (C.14), and the assumption of an adiabatic turbine, it is found that, the work comes from a total temperature drop over the turbine. Taking the mechanical efficiency η_m into account, the total temperature after the HPT T_{049} can be

calculated using equation (C.15). Next the total pressure after the HPT is calculated using equation (C.16) [1].

$$\Delta h_0 = C_P \Delta T_0 \quad \text{(C.14)}$$

$$T_{049} = T_{04} - \frac{\dot{m}_{core}\, C_{Pa}\, (T_{03} - T_{025})}{\eta_m C_{Pg}\, \dot{m}_4} \quad \text{(C.15)}$$

$$P_{049} = P_{04}\left(1 - \frac{1}{\eta_{HPT}}\left(1 - \frac{T_{049}}{T_{04}}\right)\right)^{\frac{\gamma_g}{\gamma_g - 1}} \quad \text{(C.16)}$$

The temperature and pressure drop over the LPT can be calculated in the same way which has shown in equations (C.19) and (C.20) respectively. For the LPT the work performed by the fan and booster need to be calculated as presented in equation (C.18) as the fan and booster are connected to the same shaft with LPT.

$$\dot{m}_{core} C_{Pa}(T_{013} - T_{02}) + \dot{m}_{core} C_{Pa}(T_{025} - T_{013}) = \eta_m\, \dot{m}_g C_g (T_{049} - T_{05})$$

$$C_{Pa}(T_{013} - T_{02}) + C_{Pa}(T_{025} - T_{013}) = (1 + f)\eta_m C_g (T_{049} - T_{05})$$

..... (C.18)

Where $f = \frac{\dot{m}_f}{\dot{m}_{core}}$ fuel to air ratio.

$$T_{05} = T_{049} + \frac{C_{Pa}\, (T_{013} - T_{02}) + C_{Pa}\, (T_{025} - T_{013})}{\eta_m C_{Pg}\, (1+f)} \quad \text{(C.19)}$$

$$P_{05} = P_{049}\left(1 - \frac{1}{\eta_{LPT}}\left(1 - \frac{T_{05}}{T_{049}}\right)\right)^{\frac{\gamma_g}{\gamma_g - 1}} \quad \text{(C.20)}$$

As the flow has to be expanded through both turbines, it needs to be expelled through the nozzle as assumed that the stagnation pressure and temperature are constant in the nozzle. It must be checked first if the nozzle

is choked, that is if sonic speeds are reached in the nozzle. This is true depending on if equation (C.21) is true. Here η_j is the nozzle efficiency.

$$\frac{P_{05}}{P_C} = \frac{1}{\left(1-\frac{1}{\eta_{jcore}}\left(\frac{\gamma-1}{\gamma+1}\right)\right)^{\frac{\gamma g}{\gamma g-1}}} \quad \text{(C.21)}$$

In the case of ($\frac{P_{05}}{P_C} < \frac{P_{05}}{P_a}$) the nozzle is choked, and a shockwave is present in the nozzle. In this case equations (C.22) to (C.27) are used to calculate the thrust produced by the core. The area in equation (C.26) is an approximation [5]. It is used to calculate the force caused by expanding the flow to ambient conditions outside of the engine.

$$T_9 = \frac{2T_{05}}{\gamma+1} \quad \text{(C.22)}$$

$$P_9 = P_C = \frac{P_{05}}{\frac{P_{05}}{P_C}} \quad \text{(C.23)}$$

$$v_9 = \sqrt{\gamma_g R T_9} \quad \text{(C.24)}$$

$$\rho_9 = \frac{P_9}{RT_9} \quad \text{(C.25)}$$

$$A_9 = \frac{\dot{m}_9}{\rho_9 v_9} \quad \text{(C.26)}$$

$$FN_{core} = \dot{m}_9(v_9 - v_a) + A_9(P_9 - P_a) \quad \text{(C.27)}$$

In case the nozzle is not choked, the thrust produced can be calculated using equations. (C.28) to (C.30).

$$T_9 = T_{05}\left(1 - \eta_j\left(1 - \left(\frac{P_a}{P_{05}}\right)^{\frac{\gamma g}{\gamma g-1}}\right)\right) \quad \text{(C.28)}$$

$$v_9 = \sqrt{2C_{Pg}(T_{05} - T_9)} \quad \text{(C.29)}$$

$$FN_{core} = \dot{m}_9(v_9 - v_a) \quad \text{(C.30)}$$

The thrust of the bypass flow could be calculated in the same way, again it needs to be checked if the nozzle is choked or not, as shown in equation (C.31).

$$\frac{P_{013}}{P_C} = \frac{1}{\left(1-\frac{1}{\eta_{fan}}\left(\frac{\gamma-1}{\gamma+1}\right)\right)^{\frac{\gamma_a}{\gamma a-1}}} \quad \text{(C.31)}$$

In case of bypass nozzle is choked, the equations (C.32) to (C.37) will be applied.

$$T_{19} = \frac{2T_{013}}{\gamma+1} \quad \text{(C32)}$$

$$P_{19} = P_C = \frac{P_{013}}{\frac{P_{013}}{P_C}} \quad \text{(C.33)}$$

$$v_{19} = \sqrt{\gamma_g R T_{19}} \quad \text{(C.34)}$$

$$\rho_{19} = \frac{P_{19}}{RT_{19}} \quad \text{(C.35)}$$

$$A_{19} = \frac{\dot{m_{19}}}{\rho_{19} v_{19}} \quad \text{(C.36)}$$

$$FN_{Bypass} = \dot{m_{19}}(v_{19} - v_a) + A_{19}(P_{19} - P_a) \quad \text{(C.37)}$$

In case the Bypass nozzle is not choked, the thrust produced can be calculated using equations. (C.38) to (C.40).

$$T_{19} = T_{013}\left(1 - \eta_{jbypass}\left(1 - \left(\frac{P_a}{P_{013}}\right)^{\frac{\gamma_a}{\gamma a-1}}\right)\right) \quad \text{(C.38)}$$

$$v_{19} = \sqrt{2C_{Pa}(T_{013} - T_{19})} \quad \text{(C.39)}$$

$$FN_{Bypass} = \dot{m}_{19}(v_{19} - v_a) \quad \text{(C.40)}$$

The total thrust is found by adding the core and bypass thrust as shown in equation (C.41).

$$FN = FN_{Core} + FN_{Bypass} \quad \text{(C.41)}$$

The specific Thrust is calculated by using equation (C.42).

$$Fs = \frac{\dot{m}_a}{FN} \quad \text{(C.42)}$$

The specific fuel consumption is calculated by using equation (C.43).

$$SFC = \frac{\dot{m}_f}{FN} \quad \text{(C.42)}$$